

1 PI3P dependent regulation of cell size by phosphatidylinositol 5-
2 phosphate 4-kinase

3

4

5

6

7

8

9

10 Avishek Ghosh, Aishwarya Venugopal, Dhananjay Shinde, Sanjeev Sharma, Meera Krishnan,
11 Swarna Mathre, Harini Krishnan and Padinjat Raghu

12

13 National Centre for Biological Sciences, TIFR-GKVK Campus, Bellary Road, Bangalore 560065,
14 India.

15

16 *Correspondence: praghu@ncbs.res.in

17 Tel: +91-80-23666102

18

19

20

21

22

23

24

25

26 Abstract

27 Phosphatidylinositol 3-phosphate (PI3P) and Phosphatidylinositol 5-phosphate (PI5P) are low abundant
28 phosphoinositides crucial for key cellular events such as endosomal trafficking and autophagy.
29 Phosphatidylinositol 5-phosphate 4-kinase (PIP4K) is an enzyme that regulates PI5P *in vivo* but can act on
30 both PI5P and PI3P, *in vitro*. In this study, we report a novel role for PIP4K in regulating PI3P levels in
31 *Drosophila* tissues. Loss-of-function mutants of the only PIP4K gene in *Drosophila* (*dPIP4K²⁹*) show reduced
32 cell size in larval salivary glands. We find that PI3P levels are elevated in *dPIP4K²⁹* tissues and that reverting
33 PI3P levels back towards wild type, without changes in PI5P levels, can also rescue the reduced cell size
34 phenotype. *dPIP4K²⁹* mutants also show an upregulation in autophagy and the reduced cell size can be
35 reverted by decreasing Atg8a, that is required for autophagosome maturation. Lastly, increasing PI3P levels
36 in wild type salivary glands can phenocopy the reduction in cell size and associated upregulation of
37 autophagy seen in *dPIP4K²⁹*. Thus, our study reports for the first time, a role for a PIP4K-regulated PI3P
38 pool in the control of autophagy and cell size regulation that may explain the reported role of PIP4K in
39 regulating neurodegeneration and tumour growth.

40

41

42

43

44

45

46

47

48

49

50

51

52

53 Introduction

54 The organization of membranes in eukaryotic cells is regulated by signalling mechanisms that
55 couple ongoing stimuli to sub-cellular transport mechanisms. Several signalling molecules
56 contribute to this process including proteins such as SNAREs and Rabs along with lipids.
57 Phosphoinositides are a class of signalling lipids found in all eukaryotes; they are
58 glycerophospholipids whose inositol headgroup can be phosphorylated on the 3rd, 4th or 5th
59 positions to generate molecules with signalling functions (Balla, 2013). In cells, phosphoinositides
60 are generated by the action of lipid kinases that are able to add phosphate groups to specific
61 positions on the inositol head group of specific substrates (Sasaki et al., 2009); thus the activity of
62 these lipid kinases and phosphatases is important to generate lipid signals on organelle membranes.
63 Phosphatidylinositol 5 phosphate 4-kinase (PIP4K) are one such class of lipid kinases that convert
64 phosphatidylinositol 5 phosphate (PI5P) into phosphatidylinositol 4,5 bisphosphate [PI(4,5)P₂]
65 (Clarke and Irvine, 2013; Rameh et al., 1997). Genetic analysis of *PIP4K* in various organisms
66 have demonstrated their importance in development and growth control (Gupta et al., 2013), cell
67 division (Emerling et al., 2013) immune cell function (Shim et al., 2016), metabolism (Lamia et
68 al., 2004) and neurological disorders (Al-Ramahi et al., 2017). At a cellular level, PIP4K have
69 been implicated in the control of plasma membrane receptor signalling (Sharma et al., 2019),
70 vesicular transport (Kamalesh et al., 2017), autophagy (Lundquist et al., 2018; Vicinanza et al.,
71 2015) and nuclear functions such as transcriptional control (Fiume et al., 2019). PI(4,5)P₂, the
72 product of PIP4K activity has many important functions in regulating cell physiology and
73 signalling (Kolay et al., 2016) and PI5P, the well-defined substrate of PIP4K has also been
74 implicated in regulating some sub-cellular processes (Hasegawa et al., 2017). However, despite
75 their importance in regulating several cellular processes and physiology, the biochemical reason for
76 the requirement of PIP4K in regulating these processes remain unclear.

77 When studied using biochemical activity assays *in vitro*, PIP4K shows very high activity on PI5P
78 to generate PI(4,5)P₂ (Ghosh et al., 2019; Rameh et al., 1997; Zhang et al., 1997). Coupled with
79 this, analysis of lipid levels following genetic depletion of PIP4K in various models have failed to
80 note appreciable reductions in PI(4,5)P₂ levels [reviewed in (Kolay et al., 2016)]. Rather, such
81 studies have reported an increase in the levels of the substrate, PI5P (Gupta et al., 2013; Jones et
82 al., 2006; Stijf-Bultsma et al., 2015) suggesting that the relevant biochemical function of the
83 enzyme is to regulate PI5P levels. Previous studies have noted that PIP4K depletion in *Drosophila*
84 photoreceptors (Kamalesh et al., 2017) leads to altered endocytic function and a role for PI5P in
85 regulating endocytosis has been proposed (Boal et al., 2015; Ramel et al., 2011). In mammalian
86 cells, PI5P has been proposed as a mediator of autophagy regulation by PIP4K (Al-Ramahi et al.,
87 2017; Lundquist et al., 2018; Vicinanza et al., 2015). PIP4K can also utilise PI3P as a substrate *in*
88 *vitro* (Ghosh et al., 2019; Gupta et al., 2013; Zhang et al., 1997), albeit with low efficiency;
89 however, the significance of this activity *in vivo* and the role of PIP4K, if any in regulating PI3P
90 levels *in vivo* is not known. PI3P is well known as a regulator of endocytosis and autophagy (Schink
91 et al., 2016; Wallroth and Haucke, 2018), both reported to be altered on modulating PIP4K
92 function but the significance, if any of PIP4K regulated pools of PI3P in these processes remains
93 unknown.

94

95 The *Drosophila* genome contains a single gene encoding PIP4K (*dPIP4K*). A loss-of-function allele
96 of *dPIP4K* (*dPIP4K²⁹*) results in altered growth and development, accumulation of the known
97 substrate PI5P and no reduction in PI(4,5)P₂ levels (Gupta et al., 2013). In *dPIP4K²⁹*, the size of
98 larval salivary gland cells is reduced and genetic reconstitution studies have demonstrated that the
99 kinase activity of *dPIP4K*, is required to support normal cell size (Mathre et al., 2019). Previous
100 work has shown that TORC1 signalling, a known regulator of cell size (Lloyd, 2013) and
101 autophagy (Nascimbeni et al., 2017), is reduced in *dPIP4K²⁹* (Gupta et al., 2013). Thus, while it
102 is clear that the kinase activity of *dPIP4K* is required for normal salivary gland cell size, the
103 biochemical basis for this requirement of enzyme activity is not known.

104

105 In this study, we show that in addition to the previously reported elevation of PI5P levels, PI3P
106 levels are also elevated in *dPIP4K²⁹* and this elevation in PI3P is dependent on the kinase activity
107 of dPIP4K. The reduced salivary gland cell size in *dPIP4K²⁹* could be rescued by the expression of
108 a PI3P specific 3-phosphatase, *Mtm* and this rescue was associated with a reversal of the elevated
109 PI3P but not PI5P levels. Interestingly, we observed that in larval salivary glands of *dPIP4K²⁹*, the
110 elevation in PI3P levels was associated with an upregulation in autophagy and the phenotype of
111 reduced cell size in *dPIP4K²⁹* could be reversed by down-regulating Atg8a, which functions
112 downstream to the formation of PI3P in the autophagy pathway. Elevation of PI3P levels in wild
113 type salivary glands by depletion of *Mtm* resulted in both a reduction in cell size and the enhanced
114 autophagy in salivary glands. Therefore, this study underscores a novel *in vivo* regulation of PI3P
115 levels by PIP4K in a multicellular organism leading to the control of cell size.

116

117 Results

118 *dPIP4K* does not regulate cell size through levels of its product PI(4,5)P₂

119 The kinase activity of dPIP4K is required for its ability to support salivary gland cell size (Figure 1A depicts
120 the conversion of PI5P to PI(4,5)P₂ by dPIP4K) (Mathre et al., 2019). Thus its ability to regulate cell size
121 may depend either on the elevated levels of its preferred substrate PI5P, or a shortfall in the pool of the
122 product PI(4,5)P₂ generated. Previous studies have identified a point mutation (A381E) in PIP4Kβ that
123 can switch its substrate specificity from PI5P to PI4P while still generating the same product PI(4,5)P₂
124 (Kunz et al., 2002). The corresponding point mutant version of hPIP4Kα has been used to distinguish
125 between phenotypes dependent on the PI(4,5)P₂ generated by PIP4K as opposed to PI5P metabolised by it
126 (Bulley et al., 2016). We generated a switch mutant version of human PIP4Kβ, hPIP4Kβ^[A381E] that cannot
127 utilise PI5P as a substrate but can produce PI(4,5)P₂ using PI4P as a substrate (Kunz et al., 2002).
128 Expression of hPIP4Kβ^[A381E] in the salivary glands of *dPIP4K²⁹* (*AB1> hPIP4Kβ^[A381E]; dPIP4K²⁹*) (Figure
129 S1A) did not rescue the reduced cell size whereas reconstitution with the wild type enzyme was able to do
130 so as previously reported (Figure S1Bi, quantified in Figure S1Bii, western blot in Figure S1A) (Mathre et
131 al., 2019). This observation suggests that the ability of dPIP4K to regulate cell size does not depend on the
132 pool of PI(4,5)P₂ that it generates and also that regulation of the levels of its substrate is likely to be the
133 relevant biochemical basis through which the enzyme supports cell size in salivary glands.

134

135 *Mtm* could be a candidate gene to modulate PI5P levels in *Drosophila*

136 Since PI5P is the preferred substrate of dPIP4K (Gupta et al., 2013), we sought to modulate PI5P levels to
137 assess the impact on cell size regulation. However, other biochemical players involved in PI5P regulation in
138 *Drosophila* are unknown so far. In mammals, PI5P levels are regulated by PIKFYVE, the type III PIP 5-
139 kinase that converts PI3P to PI(3,5)P₂ and PI to PI5P (Hasegawa et al., 2017; Shisheva, 2013). *Drosophila*
140 has a single PIKFYVE homologue (*CG6355*, here named *dFab1*) (Rusten et al., 2006); however, its
141 biochemical activity has not been tested (Figure 1A). We expressed mCherry tagged *dFab1* in S2R+ cells,
142 immuno-precipitated it (Figure 1Ci) and analysed its ability to phosphorylate PI3P and PI, using a LC-
143 MS/MS based *in vitro* kinase activity assay for *dFab1* (Figure 1B shows a schematic for the assay). We found
144 that the activity of *dFab1* on synthetic PI3P was approximately 4 times greater than the activity on synthetic
145 PI (Figure 1Cii). Since *dFab1* preferentially synthesizes PI(3,5)P₂ from PI3P, subsequent PI5P generation
146 would require the activity of a 3-phosphatase that can dephosphorylate PI(3,5)P₂. In mammals, *in vitro*
147 studies have revealed that lipid phosphatases of the myotubularin family have specific activity toward PI3P
148 and PI(3,5)P₂ (Figure 1A) (Laporte et al., 1996; Schaletzky et al., 2003; Walker et al., 2001). In most higher
149 order organisms, there are multiple myotubularin isoforms (Robinson and Dixon, 2006). It has been
150 suggested that *Drosophila* has six isoforms (Oppelt et al., 2013), but bioinformatic analysis using multiple
151 sequence alignment revealed that the conserved CX₅R catalytic motif is present in only 3 genes – *Mtm*,
152 *CG3632* and *CG3530* (Figure S1C). To identify the myotubularin that might generate PI5P from
153 PI(3,5)P₂, we designed a two-step *in vitro* LC-MS/MS based PI(3,5)P₂ 3-phosphatase assay using *Drosophila*
154 S2R+ cell lysates as a source of enzyme (Figure 1D, details of the assay is mentioned in methods). Briefly,
155 deuterium labelled PI(3,5)P₂ [d5-PI(3,5)P₂] is incubated with cell lysate and the PI5P formed through the
156 action of a 3-phosphatase is converted, using ¹⁸O-ATP to PI(4,5)P₂ of a unique mass owing to the
157 incorporated ¹⁸O, and subsequently detected on a mass spectrometer (Figure 1D). Each of the 3-
158 phosphatases (*Mtm*, *CG3632* and *CG3530*) were depleted using dsRNA treatment (Worby et al., 2001)
159 and the 3' phosphatase activity of the lysates were measured. We noted more than 50% knockdown using
160 dsRNA against *Mtm*, *CG3632* and *CG3530* in S2R+ cells (Figure S1Di-iii). We observed that the d5-¹⁸O-
161 PIP₂ mole fraction [the measure of PI(3,5)P₂ 3-phosphatase activity] for *Mtm* downregulated lysates was
162 significantly lower as compared to control GFP dsRNA treated lysates (Figure 1E). However, we did not
163 observe a significant difference in activity of lysates downregulated for either *CG3632* or *CG3530*.
164 Therefore, *Mtm* is a 3-phosphatase that could regulate PI5P synthesis in *Drosophila*.

165

166 ***Drosophila* Mtm reverses the cell size defect of *dPIP4K²⁹* independent of PI5P levels**

167 Based on the results of our *in vitro* results, we over-expressed *Mtm* in *dPIP4K²⁹* salivary glands to elevate
168 PI5P levels. If the reduced cell size in *dPIP4K²⁹* was linked to elevated PI5P levels, *Mtm* over-expression in
169 *dPIP4K²⁹* is expected to lead to a further reduction in cell size. Surprisingly, we observed that over-expression
170 of *Mtm* in the salivary glands of *dPIP4K²⁹* (*AB1 > MtmGFP, dPIP4K²⁹*) resulted in a reversal of cell size as
171 compared to *dPIP4K²⁹* glands (Figure 2Ai, quantified in Figure 2Aii); over-expression of the enzyme in wild
172 type salivary glands did not affect cell size (Figure S2A).

173 Mtm is a 3-phosphatase that can act on PI3P to produce PI and PI(3,5)P₂ to produce PI5P. Previously, its
174 activity on PI(3,5)P₂ has been demonstrated using purified protein in an *in vitro* phosphate-release assay
175 (Velichkova et al., 2010). To understand the biochemical basis of the ability of over-expressed Mtm to
176 reverse cell size in *dPIP4K²⁹*, we tested the biochemical activity of Mtm from *Drosophila* larval extracts using
177 our two-step 3-phosphatase activity assay. Figure 2B shows expression of C-terminus GFP tagged Mtm
178 from larval lysates at molecular weights as predicted *in silico*. We found that overexpression of Mtm did not
179 result in a statistically significant increase in 3-phosphatase activity compared to controls (Figure 2C). To
180 confirm this result was not a result of C-terminal tagging leading to Mtm inactivation, we cloned an N-
181 terminus mCherry tagged Mtm and performed the 3-phosphatase assay using S2R+ cell lysates expressing
182 mCherry_Mtm (Figure S2Bi). It was observed that a N-terminally tagged Mtm was also not active on
183 PI(3,5)P₂ as compared to controls, much like its C-terminal GFP tagged counterpart (Figure S2Bii). These
184 findings suggest that the generation of PI5P from PI(3,5)P₂ by Mtm in *Drosophila* larvae is likely to be
185 minimal. We also measured the levels of PI5P from larval lipid extracts using a recently standardised LC-
186 MS/MS based PI5P mass assay (Ghosh et al., 2019), comparing larvae expressing Mtm in *dPIP4K²⁹* mutant
187 background with *dPIP4K²⁹*. We observed that the overexpression of Mtm did not alter the levels of PI5P in
188 *dPIP4K²⁹* (Figure 2D). Therefore, together we conclude that (a) Mtm cannot synthesise PI5P from
189 PI(3,5)P₂ *in vivo* in *Drosophila* and (b) Mtm expression rescued the cell size of *dPIP4K²⁹* without changing
190 the elevated PI5P levels. Therefore, we investigated PI5P independent mechanism that control cell size.

191

192 **Mtm reduces PI3P levels when over-expressed in *dPIP4K²⁹***

193 Mtm has also been shown to dephosphorylate PI3P to generate PI *in vitro* (Velichkova et al., 2010). We
194 tested the activity of lysates expressing Mtm on synthetic PI3P using a LC-MS/MS based assay and found
195 that lysates with Mtm over-expression showed significantly higher PI3P 3-phosphatase activity compared

196 to control lysates (Figure 3A), raising the possibility that Mtm might be rescuing cell size in *dPIP4K²⁹*
197 through its PI3P 3-phosphatase activity.

198 Mtm activity can in principle change the levels of PI and PI3P; however since PI3P levels in cells are
199 substantially lower (<10%) of PI (Stephens et al., 1993), we analysed PI3P levels in relation to the ability
200 of Mtm overexpression to rescue the reduced cell size in *dPIP4K²⁹* salivary glands. Currently used methods
201 to quantify PI3P levels rely on radionuclide labelling techniques (Chicanne et al., 2012). We optimised a
202 previously used label-free LC-MS/MS based method to quantify PI3P levels from *Drosophila* larval lysates
203 [Fig 3B depicts a chromatogram derived from injecting wild type deacylated lipid samples] that allows the
204 chromatographic separation and quantification of PI3P levels (Kiefer et al., 2010). To test if the ability of
205 Mtm to dephosphorylate PI3P might be linked to its ability to reverse cell size in *dPIP4K²⁹*, we measured
206 PI3P levels in these genotypes. We observed that PI3P was significantly reduced in *dPIP4K²⁹* larvae
207 expressing Mtm compared to *dPIP4K²⁹* (Figure 3C). We also measured PI3P levels from larvae expressing
208 Mtm in an otherwise wild type background (Figure 3D) and found a modest reduction in the levels of
209 PI3P. These results highlight the potential for PI3P levels to be correlated to the phenotype of cell size
210 regulation in *Drosophila* salivary glands.

211

212 **dPIP4K regulates PI3P levels *in vivo***

213 Since reducing PI3P levels was correlated with cell size reversal in *dPIP4K²⁹* (Figure 2A and 3C), we
214 measured PI3P levels in *dPIP4K²⁹*. Interestingly, we observed that PI3P was elevated in *dPIP4K²⁹* larvae as
215 compared to controls (Figure 4A). In order to confirm this observation of elevated PI3P levels in *dPIP4K²⁹*
216 by an independent method, we devised an alternate assay to measure PI3P from larvae. Briefly, we developed
217 an *in vitro* lipid kinase reaction using purified mCherry::dFab1 to quantify PI3P from larval lipid extracts
218 using radionuclide labelling (schematic in Figure S4A). Figure 4B indicates the PI(3,5)P₂ spot on a TLC
219 formed from PI3P during the *in vitro* kinase reaction. Although lipid extracts from wild type and *dPIP4K²⁹*
220 larvae showed similar PI(3,5)P₂ spot intensities on the TLC (Figure 4B), normalisation of the PI(3,5)P₂ spot
221 intensity against total organic phosphate levels in each sample confirmed that the total PI3P levels were
222 higher in *dPIP4K²⁹* (Figure 4C) compared to controls. To confirm that the increase of PI3P in *dPIP4K²⁹*
223 was a result of the absence of PIP4K, we reconstituted wild type dPIP4K in *dPIP4K²⁹* and measured PI3P
224 (*Act5C> dPIP4KeGFP; dPIP4K²⁹*) and observed that the elevated PI3P in *dPIP4K²⁹* was reverted to normal,
225 indicating that dPIP4K can indeed regulate PI3P levels *in vivo* (Figure 4D). The catalytic activity of dPIP4K
226 is essential to maintain salivary gland cell size (Mathre et al., 2019). Therefore, to check whether this

227 catalytic activity was also necessary to control PI3P levels *in vivo*, we reconstituted *dPIP4K²⁹* with a
228 catalytically inactive dPIP4K (dPIP4K^{D271A}) and measured PI3P (*Act5C> dPIP4K^{D271A}; dPIP4K²⁹*); we found
229 that expressing catalytically dead dPIP4K^{D271A} could not significantly decrease the levels of PI3P in *dPIP4K²⁹*
230 (Figure 4E). These findings indicate that the catalytic activity of dPIP4K is required to regulate PI3P levels
231 *in vivo*.

232

233 Regulation of PI3P by dPIP4K is unlikely to be via indirect mechanisms

234 Although PI5P is the canonical *in vivo* substrate for dPIP4K, the enzyme can also use PI3P as a substrate
235 with low efficiency (Ghosh et al., 2019; Gupta et al., 2013), a feature conserved with mammalian PIP4Ks
236 (Zhang et al., 1997). In the context of our observation that PI3P levels are elevated in *dPIP4K²⁹*, dPIP4K
237 could regulate PI3P levels either through its ability to directly phosphorylate this lipid or indirectly via its
238 ability to regulate other enzymes that are established regulators of PI3P levels [e.g through negative
239 regulation of PI 3-kinase activity or through positive regulation of a 3-phosphatase that dephosphorylate
240 PI3P (Figure S4B)]. A reduction in 3-phosphatase activity on PI3P in *dPIP4K²⁹* could lead to accumulation
241 of PI3P. To test this possibility, the total 3-phosphatase activity of *dPIP4K²⁹* lysates was assessed. We did
242 not observe a reduction in 3-phosphatase activity that might explain the elevated PI3P levels. In fact, there
243 was an increase in response ratio (indicative of the 3-phosphatase activity on PI3P) in a 15 minutes *in vitro*
244 assay in mutant lysates as compared with wild type lysates (Figure 4F). In addition, we measured transcript
245 levels of three putative 3-phosphatases – *Mtm*, *CG3632* and *CG3530* and found that the transcript levels
246 of all the 3-phosphatases were unchanged in *dPIP4K²⁹* as compared to controls, although there was an overall
247 trend of decrease in all the genes (Figure 4G). PI3K59F activity could not be directly measured from larval
248 lysates; however, we measured the mRNA expression of the two known PI 3-kinase genes – *PI3K59F* and
249 *PI3K68D*. Although the transcript levels of *PI3K68D* was unchanged between *dPIP4K²⁹* and controls, we
250 observed that *PI3K59F* transcripts were in fact lower in *dPIP4K²⁹* compared to controls (Figure 4G). Thus,
251 it seems unlikely that upregulation of the aforementioned PI 3-kinases or downregulation of the 3-
252 phosphatases contributes to the increased PI3P levels in *dPIP4K²⁹*. These findings led us to conclude that
253 the regulation of PI3P levels by dPIP4K is unlikely via indirect mechanisms.

254

255 PIP4K regulates a non-endosomal PI3P pool in *Drosophila* salivary glands

256 The major source of PI3P generation in cells is the class III PI3-kinase called Vps34, whose *Drosophila*
257 ortholog is PI3K59F. PI3K59F is known to be functional at two locations in cells – namely the early

258 endosomal compartment and at multiple steps of autophagy pathway (Nascimbeni et al., 2017). In order
259 to understand the location at which PI3P is elevated in *dPIP4K²⁹*, we decided to restrict PI3K59F activity
260 to revert the increased PI3P levels at both locations of PI3K59F activity. Consequently, if PI3P at either or
261 both of these locations were relevant in regulating the cell size phenotype, we would achieve a reversal of
262 cell size by down-regulating PI3K59F in *dPIP4K²⁹* background. We down-regulated PI3K59F activity using
263 RNA interference (Figure S5A depicts the extent of *PI3K59F* transcript knockdown) in *dPIP4K²⁹*
264 background and indeed observed a reversal of cell size (Figure 5A); knockdown of *PI3K59F* in an otherwise
265 wild type background did not change cell size (Figure S5B). Further, measurement of PI3P from *dPIP4K²⁹*
266 larvae expressing PI3K59F RNAi showed a significant decrease in PI3P as compared to *dPIP4K²⁹* larvae
267 (Figure 5B).

268 To test if the early endosomal PI3P pool contributes to the reduced cell size in *dPIP4K²⁹*, we imaged the
269 tandem FYVE domain fused to mCherry (mCherry-2XFYVE), a reporter for endosomal PI3P, in salivary
270 glands of *dPIP4K²⁹* and compared it to wild type. The mCherry-2XFYVE probe revealed punctate structures
271 which were perinuclear (Figure 5Ci). Quantification of the number of punctae per unit area calculated for
272 the perinuclear sub-population showed no significant difference between wild type and *dPIP4K²⁹* salivary
273 glands (Figure 5Cii) although the probe was expressed at equal levels in both genotypes (Figure S5C). To
274 further validate if change of PI3P at the endosomal location in *dPIP4K²⁹* was correlated to the requirement
275 of dPIP4K to support cell size, we tagged dPIP4K with the tandem FYVE domain at the C-terminus end
276 of the protein (dPIP4K^{2XFYVE}) to target it to the PI3P enriched endosomal compartment and reconstituted
277 this in the background of *dPIP4K²⁹*. We did not observe a significant change in the cell size of *dPIP4K²⁹*
278 under these conditions suggesting that dPIP4K function is dispensable at this location (Figure 5D) for cell
279 size regulation.

280 The other sub-cellular location at which a Vps34-regulated PI3P pool is important, is the early
281 autophagosomal membranes. We were unable to directly measure the PI3P pool at autophagosomal
282 membranes. However, an increase in PI3P levels at this compartment would lead to an increase in the extent
283 of autophagy (Burman and Ktistakis, 2010) and can be assayed by an increase in the *Drosophila* ortholog of
284 microtubule-associated protein 1A/1B-light chain 3 (LC3) called Atg8a. We expressed mCherry::Atg8a in
285 salivary glands and the probe was expressed at equal levels in both genotypes (Figure S5D). Measurement
286 of the number of mCherry::Atg8a punctae showed a significant increase in *dPIP4K²⁹* glands compared to
287 controls (Figure 5Ei-ii), suggesting that the PI3P pool associated with the autophagy compartment is
288 upregulated in *dPIP4K²⁹*.

289

290 PIP4K in *Drosophila* salivary glands affects bulk autophagy to affect cell size

291 PI3P is formed by Vps34 and regulated by Atg1 mediated activation of the Vps34 Complex I components
292 Beclin-1 and Atg14, following which, lipidated Atg8a fuses with the formed omegasome membrane
293 containing PI3P to mature into autophagosomes (King et al., 2021). It has been demonstrated that
294 induction of autophagy by over-expressing Atg1 can cause a decrease in cell size of fat body cells in
295 *Drosophila* larvae (Scott et al., 2007). Likewise, in this study, we found that the over-expression of Atg1 in
296 the salivary glands of *Drosophila* larvae caused a drastic decrease in cell size (Figure S5E). Importantly,
297 downregulating Atg1 activity in *dPIP4K²⁹* could reverse the cell size phenotype in salivary glands while no
298 change was observed in otherwise wild type background, indicating that the autophagy pathway is
299 upregulated in *dPIP4K²⁹* (Figure S5Fi-ii). We reasoned that if the elevated PI3P in *dPIP4K²⁹* causes an
300 upregulation in autophagy leading to cell size reduction, then by down-regulating Atg8a, we would be able
301 to reverse the phenotype of cell size decrease. We indeed observed that down-regulation of Atg8a in
302 *dPIP4K²⁹* caused a reversal of the reduced cell size (Figure 5F), while there was no significant change in cell
303 size by down-regulation of Atg8a in otherwise wild type background (Figure S5G). Further, down-
304 regulation of Atg8a using the same RNAi line was able to decrease the number of mCherry::Atg8a in salivary
305 glands (Figure S5Hi-ii); the expression of the probe being equivalent between both genotypes (Figure S5I).

306

307

308 PI3P regulates cell size in salivary glands

309 We tested the effect of modulating PI3P levels in otherwise wild type salivary glands. Depletion of *Mtm*,
310 using an RNAi line has previously shown to increase PI3P levels in *Drosophila* (Jean et al., 2012; Velichkova
311 et al., 2010). Using qPCR analysis, we validated that the RNAi reagent causes specific down-regulation of
312 *Mtm* transcripts in *Drosophila* (Figure 6A). Interestingly, expressing Mtm RNAi in salivary glands caused a
313 significant decrease in cell size (Figure 6Bi and ii). Myotubularins are known to dimerize in cells and Mtm
314 harbours a C-terminal coiled-coil domain which can potentially aid in dimerization (Jean et al., 2012). We
315 observed a similar but smaller reduction in cell size when a catalytically dead version of Mtm (Mtm^{D402A}),
316 that is expected to act as dominant negative construct was expressed in salivary glands (Figure S6A). Further,
317 measurement of PI3P levels revealed a modest upregulation of PI3P levels when measured from larvae
318 expressing the Mtm RNAi (*da> Mtm RNAi*, Figure 6C). Therefore, Mtm inhibition in an otherwise
319 wildtype background can cause PI3P elevation and cell size decrease in *Drosophila*.

320 To understand if the reduction in cell size brought about by down-regulating Mtm in salivary glands causes
321 an upregulation of the autophagic pathway much like in *dPIP4K²⁹* mutants, we measured the number of
322 mCherry::Atg8a in salivary glands of Mtm RNAi (Figure 6Di). It was observed that there was a substantial
323 increase in the number of mCherry::Atg8a punctae as quantified in Figure 6Dii, although the expression of
324 the probe was expressed equivalent in both genotypes (Figure S6B). Interestingly, depleting Atg8a in salivary
325 glands also depleted of Mtm could partially rescue cell size as compared to glands where Mtm alone was
326 down-regulated (Figure 6E). These findings corroborate the relationship of increased PI3P levels to the
327 upregulation of autophagy which can eventually contribute to a decrease in cell size of salivary glands of
328 *Drosophila* larvae.

329

330 Discussion

331 Conceptually, the cellular function of any enzyme can be considered to arise from its ability to regulate the
332 levels of either the substrate or product. When PIP4K was originally described (Rameh et al., 1997), its
333 ability to generate the product PI(4,5)P₂ was recognised. However, PI(4,5)P₂, can also be synthesized from
334 phosphatidylinositol 4 phosphate (PI4P) by the activity of phosphatidylinositol 4 phosphate 5 kinase
335 (PIP5K) [reviewed in (Kolay et al., 2016)]. Since PI4P is ca.10 times more abundant than PI5P, loss of
336 PIP4K activity is unlikely to impact the overall levels of cellular PI(4,5)P₂. Consistent with this, knockout
337 of PIP4K does not reduce the overall level of PI(4,5)P₂ [(Gupta et al., 2013) discussed in (Kolay et al.,
338 2016)]. Further, a switch mutant version of PIP4K that can generate PI(4,5)P₂ from PI4P but not PI5P,
339 was unable to rescue the reduced cell size in *dPIP4K²⁹* implying that the biochemical basis of dPIP4K
340 function in supporting cell size is not its product PI(4,5)P₂. Rather, given that the kinase activity of the
341 enzyme is required for normal salivary gland cell size (Mathre et al., 2019), our findings imply that the
342 levels of the substrate are likely to be relevant. It was vital to be able to measure the levels of putative
343 substrates of PIP4K from *Drosophila* tissues and therefore, we developed a label-free LC-MS/MS based
344 methods to detect and quantify PI3P and PI5P. Previously researchers used more cumbersome radioactivity
345 based detection to measure PI3P and PI5P (Chicanne et al., 2012; Jones et al., 2013), however, new label-
346 free methods are being reported to quantify PIPs (Ghosh et al., 2019; Morioka et al., 2022). In this study,
347 we report the use of a label-free LC-MS/MS based method to measure PI3P levels *in vivo* from *Drosophila*
348 tissues for the first time. In future, this method can also be used to measure PI3P levels from tissues of other
349 model organisms to address key questions in PI3P biology.

350 Given that previous studies have identified PI5P as the substrate best utilised by PIP4K and that PI5P levels
351 are elevated in *dPIP4K²⁹*, we expected that the cell size phenotype will be mediated by PI5P levels. In the
352 course of this study, we found that (i) the expression of Mtm, a 3-phosphatase that is able to generate PI5P
353 *in vitro* from PI(3,5)P₂ rescued the reduced cell size in *dPIP4K²⁹*, (ii) The rescue of cell size in *dPIP4K²⁹* by
354 Mtm overexpression was not associated with a change in the levels of PI5P. These observations are not
355 consistent with a role for elevated PI5P levels in the reduced cell size phenotype of *dPIP4K²⁹*. Since PI3P
356 has also been shown to be a substrate of dPIP4K, albeit with less efficiency (Ghosh et al., 2019; Gupta et
357 al., 2013), we investigated PI3P levels and found that (i) PI3P levels were elevated in *dPIP4K²⁹*, (ii) were
358 reverted to wild type by reconstitution with a wild type dPIP4K transgene but not a kinase dead version,
359 (iii) the rescue of cell size in *dPIP4K²⁹* by expression of Mtm was associated with a reduction in the elevated
360 PI3P levels. Together, these findings strongly suggest that the elevated PI3P levels in *dPIP4K²⁹* underpin
361 the reduced salivary gland cell size. If elevated PI3P is a regulator of cell size, then elevation of PI3P levels
362 in wild type cells might also result in reduced cell size. Our observation that depletion of Mtm in a wildtype
363 background results in elevated PI3P levels and also reduced cell size supports this model. Overall, our data
364 supports a role for dPIP4K in the regulation of PI3P levels and cell size.

365 Interestingly, a recent study in MEFs grown in culture and downregulated of PIP4K_γ activity showed an
366 increase in PI3P and PI(3,5)P₂ levels along with an expected rise in PI5P levels (Al-Ramahi et al., 2017).
367 In mammals, the major route of synthesis of PI3P is through the action of a class III PI3-kinase called
368 Vps34. We observed that down-regulating PI3K59F, the ortholog of Vps34 in *Drosophila* reversed cell size
369 of *dPIP4K²⁹* salivary glands. These findings also identify PIP4K as a new regulator of PI3P levels along with
370 Vps34.

371 In spite of having specific stereo-chemistries, there are instances which demonstrate PI3P and PI5P to be
372 very similar to each other. The Fab1 (yeast orthologue of PIKfyve), YOTB, Vac 1 (vesicle transport
373 protein), and EEA1 (FYVE) domain has been used extensively for its lipid binding affinity for PI3P
374 (Gillooly et al., 2001). But NMR analysis revealed that FYVE domain show lesser albeit significant binding
375 affinity towards PI5P (Kutateladze et al., 1999). The Plant-Homeo-Domain (PHD) of ING2 protein,
376 which has been used in quite a few studies to probe PI5P location have revealed secondary avidities for PI3P
377 (Gozani et al., 2003). However, PIP4K_α has a less but significant *in vitro* kinase activity measured with
378 PI3P as substrate (Ghosh et al., 2019; Zhang et al., 1997). Consequently, purified *Drosophila* PIP4K also
379 shows a faint PI(3,4)P₂ spot measured through radioactive kinase assay indicating its 4-kinase activity on
380 PI3P (Gupta et al., 2013). However, due to the fold difference in *in vitro* activity between the two substrates,
381 it was never envisioned that PIP4K could regulate PI3P levels *in vivo*. Our results indicate a possibility

382 where the PIP4K can access a pool of PI3P *in vivo*, such that the enzyme achieves its optimal conditions for
383 a successful kinase reaction to metabolise PI3P.

384 What is the mechanism by which cell size is reduced in *dPIP4K²⁹*? It has been reported in several studies in
385 mammalian models that loss of PIP4K function is associated with an increase in either the initiation step
386 or flux of autophagy (Al-Ramahi et al., 2017; Lundquist et al., 2018; Vicinanza et al., 2015). Moreover, it
387 has been shown in human cells that PI5P can initiate autophagy and can even take over the function of
388 PI3P to initiate autophagy in wortmannin-treated cells (Vicinanza et al., 2015). We found that just by
389 altering PI3P levels without any change in PI5P levels, we could modify the phenotype of cell size of
390 *dPIP4K²⁹*. PI3P has been reported in primarily two cellular compartments, early endosomes and
391 autophagosomes. TORC1 activity is reported to be downregulated in *dPIP4K²⁹* (Gupta et al., 2013) and
392 consistent with the function of TORC1 in regulating autophagy, we found that levels of autophagy in
393 *dPIP4K²⁹* salivary gland cells was increased. Reducing PI3P levels by genetic knockdown of Vps34 (Class
394 III PI3K) reversed the reduced cell size phenotype in *dPIP4K²⁹* implying a role for Vps34 synthesized PI3P
395 in regulating cell size. Further, an early endosome specific dPIP4K construct could not revert the cell size
396 change of *dPIP4K²⁹*, indicating that the relevant pool of PI3P that regulates cell size is not at the early
397 endosome. Finally, inhibition of autophagy by down-regulation of Atg8a, a protein required downstream
398 of PI3P formation at the phagophore membrane during autophagosome biogenesis, in wild type results in
399 reduced cell size underscoring the requirement of normal levels of autophagy in controlling cell size in the
400 salivary gland. Additionally, we show that *Drosophila* Mtm also regulates cell size by downmodulating PI3P
401 levels and autophagy. Recent studies in *Drosophila* have identified a role for *CG3530/Mtmr6* in control of
402 basal autophagy in fat bodies (Allen et al., 2020; Manzéger et al., 2021). However, we do acknowledge that
403 Mtm downregulation does affect the endosomal PI3P pool as is reported earlier from the Kiger lab
404 (Velichkova et al., 2010). With the present data we cannot rule out an effect of endosomal PI3P in
405 contributing to cell size regulation in Mtm downregulation and perhaps the partial rescue of cell size by
406 down-regulating Atg8a explains this phenomenon (Figure 6E). Together our data provide compelling
407 evidence that the elevated levels of PI3P in *dPIP4K²⁹* induces enhanced autophagy leading to reduction in
408 cell size.

409 **Materials and methods**

410 *Fly strains and stocks*

411 All experiments were performed with *Drosophila melanogaster* (hereafter referred to as *Drosophila*). Cultures
412 were reared on standard medium containing corn flour, sugar, yeast powder and agar along with
413 antibacterial and antifungal agents. Genetic crosses were set up with Gal4 background strains and

414 maintained at 25°C and 50% relative humidity (Brand and Perrimon, 1993). There was no internal
 415 illumination within the incubator and the larvae of the correct genotype was selected at the 3rd instar
 416 wandering stage using morphological criteria. *Drosophila* strains used were Oregon-R and *w¹¹¹⁸* (wild type
 417 strain), *dPIP4K²⁹* (homozygous null mutant of dPIP4K made by Raghu lab), da-Gal4, Act5C-
 418 Gal4/CyoGFP, AB1-Gal4, UAS hPIP4K2B/TM6Tb, UAS hPIP4K2B^[A381E]/TM6Tb, Mtm^{WT}GFP (Amy
 419 Kiger, UCSD), Mtm-IR (#AK0246, Amy Kiger, UCSD), UAS dPIP4K^{WT}eGFP, UAS
 420 dPIP4K^[D271A](untagged), UAS PI3K59F RNAi (v100296, VDRC), Atg1 RNAi (44034, Bloomington),
 421 Atg8a RNAi (34340, Bloomington), *w*; UAS-*mCherry:2XFYVE²* (Amy Kiger, UCSD), UAS-mCherry-
 422 Atg8a (37750, Bloomington).

423

424 ***S2R+R+ cells: culturing and transfection***

425 *Drosophila* S2R+R+ cells were cultured and maintained as mentioned earlier (Gupta et al., 2013).
 426 Transient transfections for 48 hours were performed as mentioned previously (Mathre et al., 2019).
 427 Primers for amplifying dsRNA template against *Drosophila* genes were selected from DRSC/TRiP
 428 Functional Genomics Resources after confirming specificity of primers. A T7 RNA polymerase
 429 promoter sequence (5'-TAATACGACTCACTATAGGGAGA-3') was added at the 5' end of the
 430 primers for the T7 DNA dependent RNA polymerase to bind during *in vitro* transcription. The
 431 dsRNA was synthesised using amplicons amplified from BDGP gold clones (Mtm: LD28822,
 432 CG3632: LD11744 and CG3530: GH04637), purchased from DGRC. Following are the list of
 433 primers used for the *in vitro* transcription of dsRNA:

Primer name	Sequence
Mtm dsRNA II F (DRSC36764)	5'-TAATACGACTCACTATAGGGAGAACTCGTCGCTGGACCAGTAT-3',
Mtm dsRNA II R (DRSC36764)	5'-TAATACGACTCACTATAGGGAGAATGCGTACAAGTAGGGGGAA-3'
CG3632 dsRNA II F (DRSC36821)	5'-TAATACGACTCACTATAGGGAGAACCATCGAGAAGAATGGACG-3'
CG3632 dsRNA II R (DRSC36821)	5'- TAATACGACTCACTATAGGGAGAATAGGAACGTGCCGAAGAGA- 3'
CG3530 dsRNA I F (DRSC36794)	5'-TAATACGACTCACTATAGGGAGAGCTCGATAGCAAGGAGCACT-3'

CG3530 dsRNA I R (DRSC36794)	5'- TAATACGACTCACTATAGGGAGACAGGAGCAGGTGGTTACGTT - 3'
GFP ds RNA F	5'- TAATACGACTCACTATAGGGATGGTGAGCAAGGGCGAGGAG - 3'
GFP ds RNA R	5'- TAATACGACTCACTATAGGGCTTGTACAGCTCGTCCATGCCG - 3'

434

435 RNA extraction and qPCR analysis

436 RNA was extracted from *Drosophila* S2R+R+ cells using TRIzol reagent (15596018, Life Technologies,
 437 California, USA). Purified RNA was treated with amplification grade DNase I (18068015, Thermo Fisher
 438 Scientific, California, USA). cDNA conversion was done using SuperScript II RNase H- Reverse
 439 Transcriptase (18064014, Thermo Fisher Scientific) and random hexamers (N8080127, Thermo Fisher
 440 Scientific). Quantitative PCR (Q-PCR) was performed using Power SybrGreen PCR master-mix (4367659,
 441 Applied Biosystems, Warrington, UK) in an Applied Biosystem 7500 Fast Real Time PCR instrument.
 442 Primers were designed at the exon-exon junctions following the parameters recommended for QPCR.
 443 Transcript levels of the ribosomal protein 49 (RP49) were used for normalization across samples. Three
 444 separate samples were collected from each treatment, and duplicate measures of each sample were conducted
 445 to ensure the consistency of the data. The primers used were as follows:

446

Primer name	Sequence
Mtm Forward	5'-TAGCCAGCAGTTCAACAACG-3'
Mtm Reverse	5'-GTCTTGTGCTTGAGATCTTCCGG-3'
CG3632 Forward	5'-TGAAAAGGTTCTTTGGCCAGC-3'
CG3632 Reverse	5'- CCATTGTGTCCGCTCTGTCT - 3'
CG3530 Forward	5'-TGGACACGTCGAGCTTCATC-3'
CG3530 Reverse	5'- TCGGTAGTAGGGGTTTCAGCA- 3'
RP49 Forward	5'- CGGATCGATATGCTAAGCTGT - 3'
RP49 Reverse	5'- GCGCTTGTTTCGATCCGTA - 3'
PI3K59F Forward	5'- ACCTATTTGCTGGGTGTGGG - 3'
PI3K59F Reverse	5'- CCTTGCTCAGCTTCATTGGC - 3'
PI3K68D Forward	5'- CGAGGACTACTCCCGTGTGA - 3'
PI3K68D Reverse	5'- GTTGCTGCATCTCCGCTGTA - 3'

447 *Western blotting and immuno-precipitation*

448 **Westerns:** Salivary glands or larval samples were made exactly as mentioned in our previous work (Ghosh
449 et al., 2019; Mathre et al., 2019). Dilutions of antibodies used: 1:4000 for anti-tubulin (E7-c), (mouse)
450 from DSHB, 1:1000 for anti-mCherry antibody (Cat# PA5-34974) (Rabbit) from Thermo, 1:1000 for
451 anti-HA antibody (Cat# 2367S) (Mouse) from CST and Normal Rabbit IgG (sc-2027) from Santa Cruz.
452 **Immuno-precipitation:** About 2 million S2R+R+ cells were transfected for 48 hours and lysates were
453 prepared using 200 µl of same lysis buffer used for the preparation of protein samples for western blotting.
454 After lysis for 15 mins at 4 °C, the samples were spun down at 13000 X g for 10 mins to remove cellular
455 debris. 5% of the supernatant obtained was kept aside for input control; to the rest of the sample lysis buffer
456 was added to make up the volume to 1 mL. The volumes were split in two halves – one for IgG control and
457 the other for immune-precipitation. About 1.6 µg equivalent of antibody/normal rabbit IgG was used for
458 over-night incubation at 4 °C with continuous rotation. mCherry tagged *Drosophila* Fab1 complexes with
459 anti-mCherry antibody were precipitated by ~60 µl slurry of washed and blocked protein-G sepharose beads
460 (according to manufacturer's protocol, Sigma # GE17-0886-01) for 2 hours at 4 °C. The beads were then
461 washed with 0.1% TBST containing 0.1% 2-Mercaptoethanol, 0.1mM EGTA for two times and
462 resuspended in 100 µl of the same buffer and stored at 4 °C till kinase assay was performed.

463

464 *Cell size measurements*

465 Salivary glands were dissected from wandering third instar larvae and fixed in 4% paraformaldehyde for 20
466 min at 4°C. Post fixation, glands were washed thrice with 1X Phosphate Buffered Saline (PBS) and
467 incubated in BODIPY™ FL C12-Sphingomyelin (Cat# D7711) for 3 hours at room temperature, following
468 which they were washed thrice in 1X PBS and stained with either DAPI (Thermo Fisher, cat# D1306) or
469 TOTO3 (Thermo Fisher, cat# T3604) for 10 mins at room temperature and washed with 1X PBS again.
470 About 2-3 glands per slide were then mounted in 70% glycerol and imaged. Imaging was done on Olympus
471 FV1000 or FV3000 Confocal microscope using a 10X objective. The images were then stitched into a 3D
472 projection using an ImageJ plugin. These reconstituted 3D z stacks were then analyzed for nuclei numbers
473 (for cell number) and volume of the whole gland using Volocity Software (version 5.5.1, Perkin Elmer Inc.).
474 The average cell size was calculated as the ratio of the average volume of the gland to the number of nuclei.

475

476 *Atg8a punctae measurements*

477 Around 40 first instar larvae were picked and incubated per vial to control for crowding. Salivary glands
478 were dissected from wandering third instar larvae and fixed in 2.5% paraformaldehyde for 20 min at room
479 temperature. Post fixation, glands were washed twice with 1X PBS. Glands were mounted in 70% glycerol
480 and imaged on the same day. Imaging was done on an Olympus FV3000 Confocal microscope using a

481 60X objective. The 3D images were stitched to give one 2D image using Zproject in ImageJ. These 2D
482 images were then analysed for the number of punctae using the 3D object counter plugin in ImageJ. The
483 number of punctae were normalised to the area of the cell and plotted for the respective genotypes.

484

485 *2xFYVE punctae measurements*

486 Salivary glands were dissected and imaged as described for the ATG8a punctae measurements. The 3D
487 images were stitched to give one 2D image using Zproject in ImageJ. The 2D images were then analysed
488 for the number of punctae (analysed using 3D object counter plugin in ImageJ). The number of punctae
489 were normalised to the area of the cell and plotted for the respective genotypes.

490

491 *Lipid standards*

492 diC16-PI3P – Echelon P-3016; diC16-PI4P – Echelon P-4016; Avanti 850172 | rac-16:0 PI(3,5)P₂-d5
493 (Custom synthesised) ; 17: 0 20: 4 PI3P - Avanti LM-1900 ; 17: 0 20: 4 ; PI(4,5)P₂ - Avanti LM-1904.

494

495 *Radioactivity based PI3P mass assay*

496 diC16-PI3P (Echelon) was mixed with 20 µM Phosphatidylserine (PS) (Sigma #P5660) and dried in a
497 centrifugal vacuum concentrator. For biological samples, PS was added to the organic phase obtained at the
498 end of the neomycin chromatography before drying. To the dried lipid extracts, 50 µl 10 mM Tris-HCl
499 pH 7.4 and 50 µl diethyl ether was added and the mixture was sonicated for 2 mins in a bath sonicator to
500 form lipid micelles. The tubes were centrifuged at 1000 X g to obtain a diethyl ether phase and vacuum
501 centrifuged for 2 mins to evaporate out the diethyl ether. At this time, the reaction was incubated on ice for
502 about 10 mins and 2X kinase assay buffer (100 mM Tris pH 7.4, 20 mM MgCl₂, 140 mM KCl, and 2 mM
503 EGTA and 10 µL immuno-precipitated dFab1 bead slurry was added. To this reaction, 10 µCi [γ -³²P] ATP
504 was added and incubated at 30 °C for 16 hours. Post 16 hours, the lipids were extracted from the reaction
505 as described earlier in a radioactive PI5P mass assay protocol (Jones et al., 2013).

506

507 *Thin layer Chromatography*

508 Extracted lipids were resuspended in chloroform and resolved by TLC (preactivated by heating at 90°C for
509 1 hour) with a running solvent (45:35:8:2 chloroform: methanol: water:25% ammonia). Plates were air
510 dried and imaged on a Typhoon Variable Mode Imager (Amersham Biosciences).

511

512 *In Vitro larval lysate-based Lipid 3-phosphatase assays*

513 The assay conditions have been adopted from a previous study (Schaletzky et al., 2003). The phosphatase
514 assay comprises three parts- **(i) preparation of lysate:** third instar wandering larvae were collected in groups
515 of 5 and lysed in phosphatase lysis buffer containing 20 mM Tris-HCl (pH 7.4), 150 mM NaCl, 1% Triton
516 X-100 (v/v) and protease inhibitor cocktail (Roche), by incubating the resuspended mixture in ice for 15-
517 20 min. The larval carcasses were removed by a brief spin for 5 mins at 1000 x g speed. Total protein was
518 estimated by Bradford's reagent and desired amount of lysate was used for the subsequent assay. **(ii) Lipid**
519 **phosphatase assay:** 600 picomoles of either 17:0 20:4 PI3P or d5-PI(3,5)P₂ lipid was mixed and dried
520 with 20 µl of 0.5 M bovine brain derived Phosphatidylserine (PS) (Sigma #P5660) followed by bath
521 sonication of the mixture in presence of 50 µl of 10 mM Tris-HCl (pH 7.4) for 3 min at maximum
522 amplitude. To this 50 µl of 2× phosphatase assay buffer (Schaletzky et al., 2003) and 10 µg total protein
523 equivalents of cell free lysate was added and the reaction was incubated for 15 min at 37 °C. The reaction
524 was quenched with 125 µl of 2.4 (N) HCl followed by lipid extraction described earlier (Jones et al., 2013).
525 Samples for the PI3P assay were processed according to section (iii). For the PI(3,5)P₂ phosphatase assay
526 the dried lipids from this step were resuspended in 20 µl of 0.5 M PS and dried. To this, 50 µl of 10 mM
527 Tris-HCl (pH 7.4) was added and bath sonicated for 3 min similar to the first step of the assay. At this step,
528 50 µl of 2× kinase buffer containing 80 µM O¹⁸ ATP (OLM-7858-PK, Cambridge Isotope laboratories,
529 Inc) and 1 µg of bacterial purified human PIP4K α -GST was added and the reaction was incubated at 30
530 °C for 1 hour. This was followed by lipid extraction as described in the previous step. **(iii) Derivatization**
531 **of lipids and LC-MS/MS:** The organic phases were collected from the last step and dried and 50 µl of 2M
532 TMS-diazomethane (Acros #AC385330050) was added to each tube and vortexed gently for 10 min at
533 room temperature. The reaction was neutralized using 10 µl of glacial acetic acid. The samples were dried
534 in vacuo and 200 µl of methanol was used to reconstitute the sample to make it ready for injection for LC-
535 MS/MS analysis.

536

537 *Lipid isolation for PI5P and PI3P measurements*

538 Lipids from larvae were isolated from 3 or 5 third instar wandering larvae for PI5P or PI3P measurements,
539 respectively. Total lipids were isolated and neomycin chromatography (for PI5P measurements only) was
540 performed as described earlier (Ghosh et al., 2019).

541

542 *LC-MS/MS for in vitro assays and PI5P measurements*

543 The instrument operation was followed similar to the description in our previous methods work on PI5P
544 quantification (Ghosh et al., 2019). For *in vivo* lipid measurements, the samples were washed with post-

545 derivatisation wash step before injecting in mass spec. Samples were run on a hybrid triple quadrupole mass
546 spectrometer (Sciex 6500 Q-Trap or Sciex 5500 Q-Trap) connected to a Waters Acquity UPLC I class
547 system. Separation was performed on a ACQUITY UPLC Protein BEH C4, 300Å, 1.7 µm, 1 mm X 100
548 mm column [Product #186005590] using a 45% to 100% acetonitrile in water (with 0.1% formic acid)
549 gradient over 10 mins. MS/MS and LC conditions used were as described earlier (Ghosh et al., 2019).

550

551 *Larval PI3P measurements*

552 We adopted a previously used method of deacylation of total lipids followed by detection by LC-MS/MS
553 using ion-pairing based separation chemistry followed by detection using mass spec (Jeschke et al., 2015;
554 Kiefer et al., 2010). Using our conditions, we could not reproducibly separate the deacylated PI5P isomeric
555 peak from biological samples. But we could always separate deacylated PI3P from PI4P in these biological
556 samples (Figure 3B). Synthetic standards were used to determine the retention times of the individual
557 peaks. Figure S3A shows synthetic GroPI3P at Rt = 6.13 min and GroPI4P at Rt = 6.95 min. The Rt of
558 GroPI3P and GroPI4P was shifted in case of biological samples and in order to confirm the peaks were
559 representative of the corresponding analytes, we spiked synthetic GroPI3P into the biological sample of
560 Figure S3B. As expected, we observed a spike in the first peak, albeit at Rt = 7.65 min, without a significant
561 change in the second peak at Rt = 8.70 min, thus confirming that the first peak was indeed corresponding
562 to PI3P. Further, we also verified that GroPI3P can be linearly detected at a range of 30 - 3000 picograms
563 on column and GroPI4P can be linearly detected at a range of 30 - 4000 picograms on column (Figure S3C
564 and S3D). We determined that the Limit of detection (LOD) was 20 picograms on column for GroPI3P
565 and GroPI4P as concluded from Signal to Noise (S/N) being 30 and 24, respectively.

566 The following are the steps by which PI3P measurements were performed: **(i) Larval lipid extraction:** As
567 mentioned in previous section **(ii) lipid deacylation:** Dried lipid extracts were incubated with 1 mL of 25%
568 methylamine solution in water/methanol/n-butanol (43:46:11) at 60 °C for 1 hour followed by drying this
569 extract in vacuo (~ 3-4 hours). **(iii) fatty acid wash:** Next, the lipids were reconstituted in 40-50 µl MS-
570 grade water and to this an equal volume fatty acid extraction reagent (1-butanol/petroleum ether (40–60
571 °C boiling)/ethyl formate in a ratio of 20/4/1 (vol/vol/vol)) was added and vortexed for 2 mins. Following
572 this, the tubes were centrifuged for 5 mins at 1000 x g to obtain phase separation. The upper organic phase
573 was discarded, and the lower aqueous phase was processed for LC-MS/MS analysis.

574

575 LC-MS/MS for deacylated PI3P measurements

576 Deacylated PIPs (GroPI3P and GroPI4P) were run on a hybrid triple quadrupole mass spectrometer (Sciex
577 6500 Q-Trap) connected to a Waters Acquity UPLC I class system. Separation was performed on a
578 Phenomenex Synergi™ 2.5 µm Fusion-RP 100 Å, LC Column 100 x 2 mm, [Product # 00D-4423-B0]
579 maintained at 32°C during the run. Mobile phase A consisted of 4 mM DMHA and 5 mM acetic acid in
580 water, and mobile phase B consisted of 4 mM DMHA and 5 mM acetic acid in 100% methanol. Flow rate
581 was 0.2 mL/min.

582 The process of linear gradient elution was conducted as follows: 0–2 min (methanol, 3%), 2–5 min
583 (methanol, 7%), 5–8 min (methanol, 12%), and 8–9 min (methanol, 100%). For next 4 min, solvent B
584 was maintained at 100%. Then, equilibration was performed between 12.2 and 20.0 min using 3%
585 methanol. The injection volume and running time of each sample was 3.0 µL and 20.0 min, respectively.

586 Mass spectrometry data was acquired in multiple reaction monitoring (MRM) mode in negative polarity.
587 Quantification of PIPs was achieved with the MRM pair (Q1/Q3) m/z 413→259. Electrospray (ESI)
588 Voltage was at – 4200 V and TEM (Source Temperature) as 350 °C, DP (Declustering Potential) at -55,
589 EP (Entrance Potential) at -10, CE (Collision Energy) at -31, CXP (Collision cell Exit Potential) at -12.
590 Dwell time of 100 milliseconds was used for experiments with CAD value of -3, GS1 and GS2 at 25, CUR
591 (Curtain gas) at 40. Both Q1 and Q3 masses were scanned at unit mass resolution.

592

593 *Total Organic Phosphate measurement*

594 500 µl flow-through obtained from the phosphoinositide binding step of neomycin chromatography was
595 used for the assay for measurements of PI5P. For PI3P measurements, 50 µl was obtained from the last step
596 of lipid extraction and stored separately in phosphate free glass tubes till assay was performed. The sample
597 was heated till drying in a dry heat bath at 90°C in phosphate-free glass tubes (Cat# 14-962-26F). The rest
598 of the process was followed as described previously (Jones et al., 2013).

599

600 *Software and data analysis*

601 Image analysis was performed by Fiji software (Open source). Mass spec data was acquired on Analyst®
602 1.6.2 software followed by data processing and visualisation using MultiQuant™ 3.0.1 software and
603 PeakView® Version 2.0., respectively. Chemical structures were drawn with ChemDraw® Version 16.0.1.4.
604 Illustrations were created with BioRender.com. All datasets were statistically analysed using MS-Excel
605 (Office 2016).

606

607 Acknowledgements: This work was supported by the National Centre for Biological Sciences-TIFR
608 and a Wellcome-DBT India Alliance Senior Fellowship to PR (IA/S/14/2/501540). We thank the
609 NCBS Imaging and Mass Spectrometry Facility for support.

610

611

612 References

613 Al-Ramahi, I., Giridharan, S.S.P., Chen, Y.C., Patnaik, S., Safren, N., Hasegawa, J., de Haro, M., Gee,
614 A.K.W., Titus, S.A., Jeong, H., et al. (2017). Inhibition of PIP4K γ ameliorates the pathological effects of
615 mutant huntingtin protein. *Elife*.

616 Allen, E.A., Amato, C., Fortier, T.M., Velentzas, P., Wood, W., and Baehrecke, E.H. (2020). A conserved
617 myotubularin-related phosphatase regulates autophagy by maintaining autophagic flux. *J. Cell Biol.* 219.

618 Balla, T. (2013). Phosphoinositides: Tiny Lipids With Giant Impact on Cell Regulation. *Physiol. Rev.* 93,
619 1019–1137.

620 Boal, F., Mansour, R., Gayral, M., Saland, E., Chicanne, G., Xuereb, J.M., Marcellin, M., Burlet-Schiltz,
621 O., Sansonetti, P.J., Payrastra, B., et al. (2015). TOM1 is a PI5P effector involved in the regulation of
622 endosomal maturation. *J. Cell Sci.* 128, 815–827.

623 Brand, A.H., and Perrimon, N. (1993). Targeted gene expression as a means of altering cell fates and
624 generating dominant phenotypes. *475*, 401–415.

625 Bulley, S.J., Droubi, A., Clarke, J.H., Anderson, K.E., Stephens, L.R., Hawkins, P.T., and Irvine, R.F.
626 (2016). In B cells, phosphatidylinositol 5-phosphate 4-kinase- α synthesizes PI(4,5)P₂ to impact mTORC2
627 and Akt signaling. *Proc. Natl. Acad. Sci.* 113, 10571–10576.

628 Burman, C., and Ktistakis, N.T. (2010). Regulation of autophagy by phosphatidylinositol 3-phosphate.
629 *FEBS Lett.* 584, 1302–1312.

630 Chicanne, G., Severin, S., Boscheron, C., Terrisse, A.D., Gratacap, M.P., Gaits-Iacovoni, F., Tronchère,
631 H., and Payrastra, B. (2012). A novel mass assay to quantify the bioactive lipid PtdIns3P in various
632 biological samples. *Biochem. J.* 447, 17–23.

633 Clarke, J.H., and Irvine, R.F. (2013). Evolutionarily conserved structural changes in phosphatidylinositol
634 5-phosphate 4-kinase (PI5P4K) isoforms are responsible for differences in enzyme activity and localization.

- 635 Biochem. J. *454*, 49–57.
- 636 Emerling, B.M., Hurov, J.B., Poulogiannis, G., Tsukazawa, K.S., Choo-Wing, R., Wulf, G.M., Bell, E.L.,
637 Shim, H.S., Lamia, K.A., Rameh, L.E., et al. (2013). Depletion of a putatively druggable class of
638 phosphatidylinositol kinases inhibits growth of p53-Null tumors. *Cell* *155*, 844–857.
- 639 Fiume, R., Faenza, I., Sheth, B., Poli, A., Vidalle, M.C., Mazzetti, C., Abdul, S.H., Campagnoli, F.,
640 Fabbrini, M., Kimber, S.T., et al. (2019). Nuclear phosphoinositides: Their regulation and roles in nuclear
641 functions. *Int. J. Mol. Sci.* *20*, 1–20.
- 642 Ghosh, A., Sharma, S., Shinde, D., Ramya, V., and Raghu, P. (2019). A novel mass assay to measure
643 phosphatidylinositol-5-phosphate from cells and tissues. *Biosci. Rep.* *39*, 707604.
- 644 Gillooly, D.J., Simonsen, A., and Stenmark, H. (2001). Cellular functions of phosphatidylinositol 3-
645 phosphate and FYVE domain proteins. *Biochem. J.* *355*, 249–258.
- 646 Gozani, O., Karuman, P., Jones, D.R., Ivanov, D., Cha, J., Lugovskoy, A.A., Baird, C.L., Zhu, H., Field,
647 S.J., Lessnick, S.L., et al. (2003). The PHD finger of the chromatin-associated protein ING2 functions as
648 a nuclear phosphoinositide receptor. *114*, 99–111.
- 649 Gupta, A., Toscano, S., Trivedi, D., Jones, D.R., Mathre, S., Clarke, J.H., Divecha, N., and Raghu, P.
650 (2013). Phosphatidylinositol 5-phosphate 4-kinase (PIP4K) regulates TOR signaling and cell growth
651 during *Drosophila* development. *Proc. Natl. Acad. Sci.* *110*, 5963–5968.
- 652 Hasegawa, J., Strunk, B.S., and Weisman, L.S. (2017). PI5P and PI(3,5)P₂: Minor, but essential
653 phosphoinositides. *Cell Struct. Funct.* *42*, 49–60.
- 654 Jean, S., Cox, S., Schmidt, E.J., Robinson, F.L., and Kiger, A. (2012). Sbf/MTMR13 coordinates PI(3)P
655 and Rab21 regulation in endocytic control of cellular remodeling. *Mol. Biol. Cell* *23*, 2723–2740.
- 656 Jeschke, A., Zehethofer, N., Lindner, B., Krupp, J., Schwudke, D., Haneburger, I., Jovic, M., Backer, J.M.,
657 Balla, T., Hilbi, H., et al. (2015). Phosphatidylinositol 4-phosphate and phosphatidylinositol 3-phosphate
658 regulate phagolysosome biogenesis. *Proc. Natl. Acad. Sci.* *112*, 201423456.
- 659 Jones, D.R., Bultsma, Y., Keune, W.J., Halstead, J.R., Elouarrat, D., Mohammed, S., Heck, A.J., D’Santos,
660 C.S., and Divecha, N. (2006). Nuclear PtdIns5P as a transducer of stress signaling: an in vivo role for
661 PIP4Kbeta. *Mol. Cell* *23*, 685–695.
- 662 Jones, D.R., Ramirez, I.B.-R., Lowe, M., and Divecha, N. (2013). Measurement of phosphoinositides in
663 the zebrafish *Danio rerio*. *Nat. Protoc.* *8*, 1058–1072.

- 664 Kamalesh, K., Trivedi, D., Toscano, S., Sharma, S., Kolay, S., and Raghu, P. (2017). Phosphatidylinositol
665 5-phosphate 4-kinase regulates early endosomal dynamics during clathrin-mediated endocytosis. *J. Cell Sci.*
666 *130*, 2119–2133.
- 667 Kiefer, S., Rogger, J., Melone, A., Mertz, A.C., Koryakina, A., Hamburger, M., and Küenzi, P. (2010).
668 Separation and detection of all phosphoinositide isomers by ESI-MS. *J. Pharm. Biomed. Anal.* *53*, 552–
669 558.
- 670 King, K.E., Losier, T.T., and Russell, R.C. (2021). Regulation of Autophagy Enzymes by Nutrient
671 Signaling. *Trends Biochem. Sci.* 1–14.
- 672 Kolay, S., Basu, U., and Raghu, P. (2016). Control of diverse subcellular processes by a single multi-
673 functional lipid phosphatidylinositol 4,5-bisphosphate [PI(4,5)P₂]. *Biochem. J.* *473*, 1681–1692.
- 674 Kunz, J., Fuelling, A., Kolbe, L., and Anderson, R.A. (2002). Stereo-specific substrate recognition by
675 phosphatidylinositol phosphate kinases is swapped by changing a single amino acid residue. *J Biol Chem*
676 *277*, 5611-9.
- 677 Kutateladze, T.G., Ogburn, K.D., Watson, W.T., De Beer, T., Emr, S.D., Burd, C.G., and Overduin, M.
678 (1999). Phosphatidylinositol 3-Phosphate Recognition by the FYVE Domain The in vivo interactions
679 between FYVE domains and PtdIns(3)P are essential for the function of several pro- teins. For example,
680 EEA1 (human early endosome au. *Mol. Cell* *3*, 805–811.
- 681 Lamia, K.A., Peroni, O.D., Kim, Y.B., Rameh, L.E., Kahn, B.B., and Cantley, L.C. (2004). Increased
682 insulin sensitivity and reduced adiposity in phosphatidylinositol 5-phosphate 4-kinase beta-/- mice. *Mol*
683 *Cell Biol* *24*, 5080–5087.
- 684 Laporte, J., Hu, L.J., Kretz, C., Mandel, J.L., Kioschis, P., Coy, J.F., Klauck, S.M., Poustka, A., and Dahl,
685 N. (1996). A gene mutated in X-linked myotubular myopathy defines a new putative tyrosine phosphatase
686 family conserved in yeast. *Nat. Genet.* *13*, 175–182.
- 687 Lloyd, A.C. (2013). The regulation of cell size. *Cell* *154*, 1194–1205.
- 688 Lundquist, M.R., Goncalves, M.D., Loughran, R.M., Possik, E., Vijayaraghavan, T., Yang, A., Pauli, C.,
689 Ravi, A., Verma, A., Yang, Z., et al. (2018). Phosphatidylinositol-5-Phosphate 4-Kinases Regulate Cellular
690 Lipid Metabolism By Facilitating Autophagy. *Mol. Cell* *70*, 531-544.e9.
- 691 Manzéger, A., Tagscherer, K., Lőrincz, P., Szaker, H., Lukácsovich, T., Pilz, P., Kméczik, R., Csikós, G.,
692 Erdélyi, M., Sass, M., et al. (2021). Condition-dependent functional shift of two *Drosophila* Mtmr lipid

- 693 phosphatases in autophagy control. *Autophagy* 17, 4010–4028.
- 694 Mathre, S., Reddy, K.B., Ramya, V., Krishnan, H., Ghosh, A., and Raghu, P. (2019). Functional analysis
695 of the biochemical activity of mammalian phosphatidylinositol 5 phosphate 4-kinase enzymes. *Biosci. Rep.*
696 39, BSR20182210.
- 697 Morioka, S., Nakanishi, H., Yamamoto, T., Hasegawa, J., Tokuda, E., Hikita, T., Sakihara, T., Kugii, Y.,
698 Oneyama, C., Yamazaki, M., et al. (2022). A mass spectrometric method for in-depth profiling of
699 phosphoinositide regioisomers and their disease-associated regulation. *Nat. Commun.* 13, 1–9.
- 700 Nascimbeni, A.C., Codogno, P., and Morel, E. (2017). Phosphatidylinositol-3-phosphate in the regulation
701 of autophagy membrane dynamics. *FEBS J.* 284, 1267–1278.
- 702 Oppelt, A., Lobert, V.H., Haglund, K., Mackey, A.M., Rameh, L.E., Liestøl, K., Schink, K.O., Pedersen,
703 N.M., Wenzel, E.M., Haugsten, E.M., et al. (2013). Production of phosphatidylinositol 5-phosphate via
704 PIKfyve and MTMR3 regulates cell migration. *EMBO Rep.* 14, 57–64.
- 705 Rameh, L., Tolias, K., Duckworth, B., and Cantley, L.C. (1997). A new pathway for synthesis of
706 phosphatidylinositol- 4,5-bisphosphate. *Nature* 390, 192–196.
- 707 Ramel, D., Lagarrigue, F., Pons, V., Mounier, J., Dupuis-Coronas, S., Chicanne, G., Sansonetti, P.J., Gaits-
708 Iacovoni, F., Tronchere, H., and Payrastre, B. (2011). *Shigella flexneri* Infection Generates the Lipid PI5P
709 to Alter Endocytosis and Prevent Termination of EGFR Signaling. *Sci. Signal.* 4, ra61–ra61.
- 710 Robinson, F.L., and Dixon, J.E. (2006). Myotubularin phosphatases: policing 3-phosphoinositides. 16,
711 403–412.
- 712 Rusten, T.E., Rodahl, L.M., Pattni, K., Englund, C., Samakovlis, C., Dove, S., Brech, A., and Stenmark,
713 H. (2006). Fab1 phosphatidylinositol 3-phosphate 5-kinase controls trafficking but not silencing of
714 endocytosed receptors. *Mol Biol Cell* 17, 3989–4001.
- 715 Sasaki, T., Takasuga, S., Sasaki, J., Kofuji, S., Eguchi, S., Yamazaki, M., and Suzuki, A. (2009). Mammalian
716 phosphoinositide kinases and phosphatases. *Prog. Lipid Res.* 48, 307–343.
- 717 Schaletzky, J., Dove, S.K., Short, B., Lorenzo, O., Clague, M.J., and Barr, F. a (2003).
718 Phosphatidylinositol-5-phosphate activation and conserved substrate specificity of the myotubularin
719 phosphatidylinositol 3-phosphatases. *Curr. Biol.* 13, 504–509.
- 720 Schink, K.O., Tan, K.-W., and Stenmark, H. (2016). Phosphoinositides in Control of Membrane
721 Dynamics. *Annu. Rev. Cell Dev. Biol.* 32, 143–171.

- 722 Scott, R.C., Juhász, G., and Neufeld, T.P. (2007). Direct Induction of Autophagy by Atg1 Inhibits Cell
723 Growth and Induces Apoptotic Cell Death. *Curr. Biol.* *17*, 1–11.
- 724 Sharma, S., Mathre, S., Ramya, V., Shinde, D., and Raghu, P. (2019). Phosphatidylinositol 5 Phosphate
725 4-Kinase Regulates Plasma-Membrane PIP3 Turnover and Insulin Signaling. *Cell Rep.* *27*, 1979–1990.e7.
- 726 Shim, H., Wu, C., Ramsamooj, S., Bosch, K.N., Chen, Z., Emerling, B.M., Yun, J., Liu, H., Choo-Wing,
727 R., Yang, Z., et al. (2016). Deletion of the gene *Pip4k2c*, a novel phosphatidylinositol kinase, results in
728 hyperactivation of the immune system. *Proc. Natl. Acad. Sci.* *113*, 7596–7601.
- 729 Shisheva, A. (2013). PtdIns5P: News and views of its appearance, disappearance and deeds. *Arch. Biochem.*
730 *Biophys.*
- 731 Stephens, L.R., Jackson, T.R., and Hawkins, P.T. (1993). Agonist-stimulated synthesis of
732 phosphatidylinositol(3,4,5)-trisphosphate. A new intracellular signalling system? *BBA - Mol. Cell Res.*
733 *1179*, 27–75.
- 734 Stijf-Bultsma, Y., Sommer, L., Tauber, M., Baalbaki, M., Giardoglou, P., Jones, D.R., Gelato, K.A., van
735 Pelt, J., Shah, Z., Rahnamoun, H., et al. (2015). The Basal Transcription Complex Component TAF3
736 Transduces Changes in Nuclear Phosphoinositides into Transcriptional Output. *Mol. Cell* *58*, 453–467.
- 737 Velichkova, M., Juan, J., Kadandale, P., Jean, S., Ribeiro, I., Raman, V., Stefan, C., and Kiger, A.A. (2010).
738 *Drosophila* Mtm and class II PI3K coregulate a PI(3)P pool with cortical and endolysosomal functions. *J.*
739 *Cell Biol.* *190*, 407–425.
- 740 Vicinanza, M., Korolchuk, V.I., Ashkenazi, A., Puri, C., Menzies, F.M., Clarke, J.H., and Rubinsztein,
741 D.C. (2015). PI(5)P regulates autophagosome biogenesis. *Mol. Cell* *57*, 219–234.
- 742 Walker, D.M., Urbé, S., Dove, S.K., Tenza, D., Raposo, G., Clague, M.J., Urbe, S., Dove, S.K., Tenza,
743 D., Raposo, G., et al. (2001). Characterization of MTMR3. an inositol lipid 3-phosphatase with novel
744 substrate specificity. *Curr. Biol.* *11*, 1600–1605.
- 745 Wallroth, A., and Haucke, V. (2018). Phosphoinositide conversion in endocytosis and the endolysosomal
746 system. *J. Biol. Chem.* *293*, 1526–1535.
- 747 Worby, C.A., Simonson-Leff, N., and Dixon, J.E. (2001). RNA interference of gene expression (RNAi) in
748 cultured *Drosophila* cells. *Sci. STKE* *2001*, 1–9.
- 749 Zhang, X., Loijens, J.C., Boronenkov, I. V, Parker, G.J., Norris, F.A., Chen, J., Thum, O., Prestwich,
750 G.D., Majerus, P.W., and Anderson, R.A. (1997). Phosphatidylinositol-4-phosphate 5-kinase isozymes

751 catalyze the synthesis of 3-phosphate-containing phosphatidylinositol signaling molecules. J. Biol. Chem.
752 272, 17756–17761.

753

754

755

756

757

758

759

760

761

762 Figure legends:

763 Figure 1: Screening for a biochemical route to modulate PI5P levels in *Drosophila* as altering local
764 PI(4,5)P₂ couldn't change cell size of *dPIP4K*²⁹

765 (A) Schematic illustrating the putative enzymatic routes by which PI5P can be synthesised in *Drosophila*.
766 The activities of enzymes labelled in blue are known in mammalian cells, the activity of enzymes
767 labelled in red followed by “?” are still unknown in *Drosophila*, the activity of enzymes labelled in
768 green are known in *Drosophila*. The activity of PI5P to PI(4,5)P₂ is boxed and is linked to cell size
769 regulation in *Drosophila* (Mathre et al., 2019). PI: Phosphatidylinositol, PI3P: Phosphatidylinositol
770 3-phosphate, PI(3,5)P₂: Phosphatidylinositol 3,5 bisphosphate, PI5P: Phosphatidylinositol 5-
771 phosphate, PI(4,5)P₂: Phosphatidylinositol 4,5 bisphosphate.

772 (B) Schematic illustrating the LC-MS/MS based *in vitro* 5-kinase activity assay using S2R+ cells over-
773 expressing dFab1 enzyme to convert synthetic PI or PI3P to PI5P and PI(3,5)P₂, respectively.

774 (C) (i) Immunoprecipitated protein levels were analysed by Western blotting with an anti-mCherry
775 antibody. Control (IgG) was prepared without anti-mCherry. Input lane shows the correct size of
776 dFab1 protein ~230 kDa. UTC: Untransfected control.

777 (ii) *In vitro* kinase assay on synthetic PI and PI3P. Graph representing the Kinase activity (%) as the
778 normalised response ratio of “PI 5-kinase activity on PI” to “PI3P 5-kinase activity on PI3P” upon
779 enzymatic activity of immunoprecipitated mCherry::dFab1 on the respective substrates. Response ratio
780 of PI 5-kinase activity on PI is obtained from area under the curve (AUC) of 17:0 14:1 PI5P
781 (Product)/17:0 14:1 PI (Substrate), Response ratio of PI3P 5-kinase activity on PI3P is obtained from
782 area under the curve (AUC) of 17:0 20:4 PI(3,5)P₂ (Product)/17:0 20:4 PI3P (Substrate) and is
783 represented as mean ± S.E.M. on addition of either negative control (no beads), Control (mCherry
784 beads) or dFab1 (mCherry::dFab1 beads). Number of immunoprecipitated samples = 2.

785 (D) Schematic illustrating the LC-MS/MS based *in vitro* PI(3,5)P₂ 3-phosphatase activity assay using
786 dsRNA treated S2R+ cells as enzyme source to convert synthetic PI(3,5)P₂ [d5-PI(3,5)P₂ to d5-¹⁸O-
787 PIP₂] using a two-step reaction scheme.

788 (E) *In vitro* phosphatase assay on synthetic PI(3,5)P₂. Graph representing the 3-Phosphatase activity
789 (%) as the percent formation of d5-¹⁸O-PIP₂ formed from starting d5-PI(3,5)P₂ as mean ± S.E.M.
790 on addition of either control (GFP ds RNA) or Mtm, CG3632, CG3530 ds RNA treated S2R+ cell
791 lysates. One way ANOVA with a post hoc Tukey’s test shows p value = 0.003 between GFP and
792 Mtm ds RNA treated lysates, shows p value = 0.63 between GFP and CG3632 ds RNA treated
793 lysate and shows p value = 0.11 between GFP and CG3530 ds RNA treated lysates.

794 Supporting Figure 1: Fab1 and Mtm can are potential PI5P modulating enzymes in *Drosophila*

795 (A) Protein levels between AB1Gal4/+ ; *dPIP4K²⁹* (Ctl), AB1 >hPIP4KB2::GFP ; *dPIP4K²⁹* and, AB1
796 >hPIP4KB2^{A381E}::GFP; *dPIP4K²⁹* from salivary glands of third instar wandering larvae seen on a
797 Western blot probed by GFP antibody. Both hPIP4KB2::GFP and hPIP4KB2^{A381E}::GFP migrates
798 ~75 kDa. Actin was used as the loading control.

799 (B)

800 (i) Representative confocal images of salivary glands from the genotypes a. *AB1/+ ; dPIP4K²⁹*
801 , b. *AB1>hPIP4Kβ; dPIP4K²⁹*, c. *AB1>hPIP4Kβ^{[A381E]; dPIP4K²⁹}*. Cell body is marked
802 majenta by BODIPY conjugated lipid dye, nucleus is marked by TOTO-3 shown in green.
803 Scale bar indicated at 100 μm.

804 (ii) Graph representing average cell size measurement (in μm³) as mean ± S.E.M. of salivary
805 glands from wandering third instar larvae of *AB1/+; dPIP4K²⁹* (n = 9), *AB1>hPIP4Kβ;*
806 *dPIP4K²⁹* (n = 8), *AB1>hPIP4Kβ^{[A381E]; dPIP4K²⁹}* (n = 6). Sample size is represented on
807 individual bars. One way ANOVA with post hoc Tukey’s test showed p value = 0.0002

808 between *AB1/+; dPIP4K²⁹* and *AB1>hPIP4K β ; dPIP4K²⁹* and p value = 0.379 between
809 *AB1/+; dPIP4K²⁹* and *AB1>hPIP4K β ^[A381E]; dPIP4K²⁹*.

810 (C) Multiple sequence alignment of the myotubularin phosphatase family proteins in *Drosophila* with
811 human myotubularins share a common signature phosphatase catalytic motif, the C(X₅)R motif
812 (highlighted in red box) except *CG5026*, *CG14411*. The alignment was generated using clustalO
813 and representation is using Jalview. Conservation is shown in range of white to black, black being
814 most conserved.

815

816 (D) (i) qPCR measurements for mRNA levels of *Mtm*, *CG3632* and *CG3530* from either *GFP* ds RNA
817 (green) or *Mtm* ds RNA treated samples (magenta). Student's unpaired t-test showed p value =
818 0.009 between *GFP* ds RNA and *Mtm* ds RNA for *Mtm*, while p value = 0.36, p value = 0.46 for
819 genes *CG3632* and *CG3530*, respectively.

820 (ii) qPCR measurements for mRNA levels of *Mtm*, *CG3632* and *CG3530* from either *GFP* ds
821 RNA (green) or *CG3632* ds RNA treated samples (magenta). Student's unpaired t-test showed p
822 value = 0.02 between *GFP* ds RNA and *CG3632* ds RNA for *CG3632*, while p value = 0.29, p
823 value = 0.46 for genes *Mtm* and *CG3530*, respectively.

824 (iii) qPCR measurements for mRNA levels of *Mtm*, *CG3632* and *CG3530* from either *GFP* ds
825 RNA (green) or *CG3530* ds RNA treated samples (magenta). Student's unpaired t-test showed p
826 value = 0.0008 between *GFP* ds RNA and *CG3530* ds RNA for *CG3530*, while p value = 0.97, p
827 value = 0.31 for genes *Mtm* and *CG3632*, respectively.

828 **Figure 2: *Drosophila* Mtm rescues the cell size defect of *dPIP4K²⁹* independent of PI5P levels**

829 (A) (i) Representative confocal images of salivary glands from the genotypes a. *AB1/+ ; dPIP4K²⁹*,
830 b. *AB1>Mtm^{WT}GFP ; dPIP4K²⁹*. Cell body is marked magenta by BODIPY conjugated lipid dye,
831 nucleus is marked by TOTO-3 shown in green. Scale bar indicated at 50 μ m.

832 (ii) Graph representing average cell size measurement (in percentage) as mean \pm S.E.M. of
833 salivary glands from wandering third instar larvae of *AB1/+ ; dPIP4K²⁹* (n = 8),
834 *AB1>Mtm^{WT}GFP ; dPIP4K²⁹* (n = 8). Sample size is represented on individual bars.
835 Student's unpaired t-test with Welch correction showed p value = 0.003 between *AB1/+ ;*
836 *dPIP4K²⁹* and *AB1>Mtm^{WT}GFP ; dPIP4K²⁹*.

837

838 (B) Protein levels between *daGal4/+* (Ctl) and *da> Mtm^{WT}GFP* from third instar wandering larvae seen
839 on a Western blot probed by GFP antibody. *Mtm^{WT}GFP* migrates ~100 kDa. Tubulin was used as
840 the loading control.

841 (C) *In vitro* phosphatase assay on synthetic PI(3,5)P₂. Graph representing the formation of ¹⁸O-PIP₂
842 formed from starting PI(3,5)P₂ as substrate represented as mean ± S.E.M. on addition of either
843 control (*da/+*) or *da>Mtm_GFP* lysates. Lysate samples n = 3, where each sample was made from
844 five third instar wandering larvae. Student's unpaired t-test with Welch correction showed p value
845 = 0.23.

846 (D) Graph representing Normalised PI5P levels which is total ¹⁸O-PIP₂/peak area of 17:0 20:4 PI(4,5)P₂
847 (internal standard) normalised to organic phosphate value as mean ± S.E.M. of *da/+ ; dPIP4K²⁹*
848 (green) or *da> Mtm^{WT}GFP, dPIP4K²⁹* (magenta). Biological samples n = 3, where each sample was
849 made from five third instar wandering larvae. Unpaired t test with Welch's correction showed p
850 value = 0.7830 between *da/+ ; dPIP4K²⁹* and *da> Mtm^{WT}GFP, dPIP4K²⁹*.

851

852 **Supporting Figure 2: *Drosophila* Mtm rescues the cell size defect of *dPIP4K²⁹* independent of PI5P**
853 **levels**

854 (A) Graph representing average cell size measurement (in percentage) as mean ± S.E.M. of salivary
855 glands from wandering third instar larvae of *AB1/+* (n = 8) and *AB1>Mtm^{WT}GFP* (n = 8). Sample
856 size is also represented by points on individual bars. Student's unpaired t-test with Welch correction
857 showed p value = 0.392.

858 (B) (i) Protein levels between lysates made from *Drosophila* S2R+ cells. Lanes from left: untransfected
859 control (UTC), mCherry vector and mCherry_Mtm observed on a Western blot probed by
860 mCherry antibody. mCherry_Mtm migrates ~100 kDa. Tubulin was used as the loading control.

861 (ii) *In vitro* phosphatase assay on synthetic PI(3,5)P₂. Graph representing the formation of ¹⁸O-
862 PIP₂ formed from starting PI(3,5)P₂ as substrate represented as mean ± S.E.M. on addition of either
863 control (mCherry vector transfected lysates) or mCherry_Mtm lysates. Lysate samples n = 3, where
864 each sample was made from five third instar wandering larvae. Student's unpaired t-test with Welch
865 correction showed p value = 0.696.

866

867 **Figure 3: Mtm reduces PI3P levels when over-expressed in *dPIP4K²⁹***

- 868 (A) *In vitro* phosphatase assay on synthetic PI3P. Graph representing the response ratio of 17:0 20:4
869 PI (Product)/17:0 20:4 PI3P (Substrate) formed as mean \pm S.E.M. on addition of either control
870 (da/+) or da>Mtm^{WT}GFP lysates. Lysate samples = 3, where each sample was made from five third
871 instar wandering larvae. Student's unpaired t-test with Welch correction showed p value = 0.007.
- 872 (B) Extracted ion chromatogram (XIC) of deacylated PI3P or GroPI3P (Glycerophosphoinositol 3-
873 phosphate) peak at Rt = 7.37 min, separated from deacylated PI4P or GroPI4P
874 (Glycerophosphoinositol 4-phosphate) peak at Rt = 9.12 min obtained from injecting wild type
875 larval lipid extract (details of sample preparation is discussed in methods).
- 876 (C) Graph representing Normalised PI3P levels which is the peak area of GroPI3P/ peak area of
877 GroPI4P normalised to organic phosphate value of total lipid extracts as mean \pm S.E.M. of da/+ ;
878 *dPIP4K²⁹* (green) and da> Mtm^{WT}GFP, *dPIP4K²⁹* (majenta). Biological samples = 3, where each
879 sample was made from three third instar wandering larvae. Student's unpaired t-test with Welch
880 correction showed p value = 0.07.
- 881 (D) Graph representing Normalised PI3P levels which is the peak area of GroPI3P/ peak area of
882 GroPI4P normalised to organic phosphate value of total lipid extracts as mean \pm S.E.M. of da/+
883 (green) and da> Mtm^{WT}GFP, (majenta). Biological samples = 3, where each sample was made from
884 three third instar wandering larvae. Student's unpaired t-test with Welch correction showed p value
885 = 0.13.

886

887

888

889 Supporting Figure 3: Mtm reduces PI3P levels when over-expressed in *dPIP4K²⁹*

- 890 (A) XIC obtained from a mixture of synthetic GroPI3P and GroPI4P standard mixture at 300
891 picograms on column eluting at Rt = 6.13 min and Rt = 6.95 min, respectively.
- 892 (B) XIC obtained from a biological sample spiked with 200 picograms of synthetic GroPI3P, eluting
893 at Rt = 7.65 min and GroPI4P eluting at Rt = 8.70 min, respectively. The area under the curve
894 (AUC) for GroPI3P changed by 29 times whereas the AUC of GroPI4P changed by 1.5 times,
895 indicating that the first peak obtained in biological samples is indeed GroPI3P.

896 (C) A dose–response curve of synthetic GroPI3P ranging from 30 to 3000 picograms on column. Y-
897 axis depicts intensity of GroPI3P (in cps) and X-axis represents the amount of GroPI3P loaded on
898 column. Equation: $y = 93.704x - 7243.1$; $R^2 = 0.9964$.

899 (D) A dose–response curve of synthetic GroPI4P ranging from 30 to 4000 picograms on column. Y-
900 axis depicts intensity of GroPI4P (in cps) and X-axis represents the amount of GroPI4P loaded on
901 column. Equation: $y = 212.49x - 505.82$; $R^2 = 0.9999$.

902

903 **Figure 4: dPIP4K regulates PI3P levels *in vivo***

904 (A) Graph representing Normalised PI3P levels which is the peak area of GroPI3P/ peak area of
905 GroPI4P normalised to organic phosphate value as mean \pm S.E.M. of wild type (green) and
906 *dPIP4K²⁹* (majenta). Biological samples = 5, where each sample was made from five third instar
907 wandering larvae. Unpaired t-test with Welch correction showed p value = 0.008.

908 (B) Autoradiograph of TLC ran with lipid samples from *in vitro* PI3P mass assay using wild type (WT)
909 and *dPIP4K²⁹* lipid samples. The first two lanes from the left are obtained from mass assay reactions
910 using synthetic PI3P standard without or with addition of dFab1 enzyme, respectively. The origin
911 spot and PI(3,5)P₂ spots are marked.

912 (C) The graph represents normalised PI3P levels. Briefly, the spot marked as PI(3,5)P₂ on TLC in (B)
913 is obtained by converting PI3P in the samples using immunoprecipitated dFab1 in presence of
914 γ ³²P-ATP are quantified using image analysis and then normalised to organic phosphate value
915 (indicated in blue embedded text under TLC) to obtain normalised PI3P levels. Biological samples
916 = 3, where each sample was made from five third instar wandering larvae. **Student's unpaired** t-test
917 with Welch correction showed p value = 0.036.

918 (D) Graph representing Normalised PI3P levels which is the peak area of GroPI3P/ peak area of
919 GroPI4P normalised to organic phosphate value of total lipid extracts as mean \pm S.E.M. of
920 Act5C/+; *dPIP4K²⁹* (green), or Act5C> dPIP4K^{WT}GFP, *dPIP4K²⁹* (majenta). Biological samples =
921 5, where each sample was made from three third instar wandering larvae. **Student's unpaired** t-test
922 with Welch correction showed p value = 0.008.

923 (E) Graph representing Normalised PI3P levels which is the peak area of GroPI3P/ peak area of
924 GroPI4P normalised to organic phosphate value of total lipid extracts as mean \pm S.E.M. of Act5C/+
925 ; *dPIP4K²⁹* (green) or Act5C> dPIP4K^{D271A}, *dPIP4K²⁹* (majenta). Biological samples = 6, where

926 each sample was made from three third instar wandering larvae. Student's unpaired t-test with
927 Welch correction showed p value = 0.818.

928 (F) *In vitro* phosphatase assay on synthetic PI3P. Graph representing the response ratio of 17:0 20:4
929 PI (Product)/17:0 20:4 PI3P (Substrate) formed as mean \pm S.E.M. on addition of either wildtype
930 (WT) or *dPIP4K²⁹* lysates for either a 5 min or a 15 min reaction. Lysate samples = 3, where each
931 sample was made from five third instar wandering larvae. Multiple unpaired t-test showed p value
932 = 0.26 for 5 min time point and p value = 0.052.

933 (G) qPCR measurements for mRNA levels of *PI3K59F* and *PI3K68D* from either Wild type (green)
934 or *dPIP4K²⁹* (magenta). Student's unpaired t-test showed p value = 0.01 for *PI3K59F* and p value
935 = 0.58 for *PI3K68D*. qPCR measurements for mRNA levels of *Mtm*, *CG3632* and *CG3530* from
936 either Wild type (green) or *dPIP4K²⁹* (magenta). Student's unpaired t-test showed p value = 0.03
937 for *Mtm*, p value = 0.23 for *CG3632* and p value = 0.0006 for *CG3530*.

938

939 Supporting Figure 4: *Drosophila* PIP4K regulates *in vivo* PI3P levels

940 (A) Schematic illustrating the methodology to assay PI3P by a dFab1 mediated radioactivity-based
941 mass assay. dFab1 is purified from S2R+ cells by immunoprecipitation and used to convert PI3P
942 from total lipid extracts obtained from larvae in presence of γ ³²P-ATP to radiolabelled PI(3,5)P₂
943 product which is finally analysed using thin layer chromatography (TLC). A portion of the total
944 lipid extract is used for organic phosphate assay to normalise for sample size.

945 (B) Illustration depicting a model where the increased PI3P levels in *dPIP4K²⁹* can be explained by
946 either an activation of PI 3-kinase activity (green arrow) or an inhibition of PI3P 3-phosphatase
947 activity (red stubbed arrow).

948

949

950

951 Figure 5: PIP4K in *Drosophila* salivary glands affects bulk autophagy to affect cell size

952 (A) Graph representing average cell size measurement (in μm^3) as mean \pm S.E.M. of salivary glands
953 from wandering third instar larvae of *AB1/+*; *dPIP4K²⁹* (n = 9), *AB1>PI3K59F RNAi*; *dPIP4K²⁹*

954 (n = 9). Sample size is represented on individual bars. Student's unpaired t-test with Welch
955 correction showed p value <0.0001.

956 (B) Graph representing Normalised PI3P levels which is the peak area of GroPI3P/ peak area of
957 GroPI4P normalised to organic phosphate value of total lipid extracts as mean \pm S.E.M. of Act5C/+
958 ; *dPIP4K²⁹* (green), or Act5C> *dPIP4K^{WT}GFP*, *dPIP4K²⁹* (magenta). Biological samples = 5, where
959 each sample was made from five third instar wandering larvae. Student's unpaired t-test with Welch
960 correction showed p value = 0.011.

961 (C) (i) Representative confocal z-projections depicting a sub population of early endosomal
962 compartment using 2xFYVE-mCherry in the salivary glands from wandering third instar larvae of
963 *AB1> 2xFYVE-mCherry* and *AB1> 2xFYVE-mCherry ; dPIP4K²⁹*. Scale bar indicated at 20 μ m.

964 (ii) Graph representing 2xFYVE punctae measurement in the salivary glands from wandering third
965 instar larvae of *AB1> 2xFYVE-mCherry* (N = 8, n=40) and *AB1> 2xFYVE-mCherry; dPIP4K²⁹* (N
966 =8, n = 40). Student's unpaired t-test with Welch correction showed p value = 0.4057

967 (D) Graph representing average cell size measurement (in μ m³) as mean \pm S.E.M. of salivary glands
968 from wandering third instar larvae of *AB1/+ ; dPIP4K²⁹* (n = 8), *AB1>dPIP4K^{2xFYVE} ; dPIP4K²⁹* (n
969 = 8). Sample size is represented on individual bars. Student's unpaired t-test with Welch correction
970 showed p value = 0.171.

971 (E) (i) Representative confocal z-projections depicting autophagosomal levels using Atg8a-mCherry in
972 the salivary glands from the wandering third instar larvae of *AB1>ATG8a-mCherry* and
973 *AB1>ATG8a-mCherry; dPIP4K²⁹*. Scale bar indicated at 20 μ m.

974 (ii) Graph representing Atg8a punctae measurement in the salivary glands from wandering third
975 instar larvae of *AB1>ATG8a-mCherry* (N = 10, n = 60) and *AB1>ATG8a-mCherry; dPIP4K²⁹* (N
976 = 10, n = 62). Student's unpaired t-test with Welch correction showed p value <0.0001.

977 (F) Graph representing average cell size measurement (in μ m³) as mean \pm S.E.M. of salivary glands
978 from wandering third instar larvae of *AB1/+ ; dPIP4K²⁹* (n = 9), *AB1>PI3K59F RNAi ; dPIP4K²⁹*
979 (n = 9). Sample size is represented on individual bars. Student's unpaired t-test with Welch
980 correction showed p value <0.0001.

981

982 Supporting Figure 5: PIP4K in *Drosophila* salivary glands affects bulk autophagy to affect cell size

- 983 (A) qPCR measurements for mRNA levels of *PI3K59F* and *PI3K68D* from either Control
984 (*Act5C/+*, green) or *Act5C > PI3K59F* RNAi (magenta). Multiple t-test with post hoc Holm-
985 Sidak's test showed p value < 0.0001 between *Act5C/+* and *Act5C > PI3K59F* RNAi for
986 *PI3K59F* and p value = 0.62 between *Act5C/+* and *Act5C > PI3K59F* RNAi for *PI3K68D*.
- 987 (B) Graph representing average cell size measurement (in μm^3) as mean \pm S.E.M. of salivary glands
988 from wandering third instar larvae of *AB1/+* (n = 12), *AB1 > PI3K59F* RNAi (n = 9). Sample
989 size is represented on individual bars. Student's unpaired t-test with Welch correction showed
990 p value = 0.55.
- 991 (C) Immunoblot from the salivary glands of wandering third instar larvae probed using mCherry
992 antibody showing expression of 2xFYVE-mCherry in *AB1 > 2xFYVE-mCherry* (control) and
993 *AB1 > 2xFYVE-mCherry ; dPIP4K²⁹*. 2xFYVE-mCherry migrates ~50 kDa. Actin was used as
994 the loading control. dPIP4K protein was checked in the samples to ascertain the mutant
995 background.
- 996 (D) Immunoblot from the salivary glands of wandering third instar larvae probed using mCherry
997 antibody showing expression of Atg8a-mCherry in *AB1 > ATG8amCherry* (control) and
998 *AB1 > ATG8amCherry ; dPIP4K²⁹*. Atg8a-mCherry migrates ~42 kDa. Tubulin was used as the
999 loading control. dPIP4K protein was checked in the samples to ascertain the mutant
1000 background.
- 1001 (E) Graph representing average cell size measurement (in μm^3) as mean \pm S.E.M. of salivary glands
1002 from wandering third instar larvae of *AB1/+* (n = 3), *AB1 > Atg1* (n = 2). Sample size is
1003 represented on individual bars. Statistical test not performed.
- 1004 (F) (i) Graph representing average cell size measurement (in μm^3) as mean \pm S.E.M. of salivary
1005 glands from wandering third instar larvae of *AB1/+* (n = 12), *AB1 > Atg1* RNAi (n = 10).
1006 Sample size is represented on individual bars. Student's unpaired t-test with Welch correction
1007 showed p value = 0.92.
- 1008 (ii) Graph representing average cell size measurement (in μm^3) as mean \pm S.E.M. of salivary
1009 glands from wandering third instar larvae of *AB1/+ ; dPIP4K²⁹* (n = 11), *AB1 > Atg1* RNAi
1010 ; *dPIP4K²⁹* (n = 9). Sample size is represented on individual bars. Student's unpaired t-test
1011 with Welch correction showed p value < 0.0001.

1012 (G) Graph representing average cell size measurement (in μm^3) as mean \pm S.E.M. of salivary glands
1013 from wandering third instar larvae of *AB1/+* (n = 9), *AB1>Atg8a* RNAi (n = 8). Sample size is
1014 represented on individual bars. Student's unpaired t-test with Welch correction showed p value
1015 = 0.67.

1016 (H) (i) Representative confocal z-projections depicting autophagosomal levels using Atg8a-
1017 mCherry in the salivary glands from the genotypes a. *AB1>ATG8a-mCherry*, b. *AB1>ATG8a-*
1018 *mCherry ; ATG8aRNAi*. Scale bar indicated at 20 μm .

1019 (ii) Graph representing Atg8a punctae measurement in the salivary glands from wandering
1020 third instar larvae of *AB1>ATG8a-mCherry* (N =8 , n =40) and *AB1>ATG8a-mCherry ;*
1021 *ATG8aRNAi* (N =8 ,n =40). Student's unpaired t-test with Welch correction showed p
1022 value = 0.0197.

1023 (i) Immunoblot from the salivary glands of wandering third instar larvae probed using mCherry
1024 antibody showing the expression of Atg8a-mCherry in *AB1>ATG8amCherry* (control) and
1025 *AB1>ATG8a-mCherry ; ATG8aRNAi*. Atg8a-mCherry migrates \sim 42 kDa. Actin was used as
1026 the loading control.

1027

1028 Figure 6: PI3P regulates cell size In salivary glands

1029 (A) qPCR measurements for mRNA levels of *mtm*, *CG3632* and *CG3530* from either Control
1030 (*daGal4/+*, in green) or *da> Mtm* RNAi, in majenta. Multiple t-test with post hoc Holm-Sidak's
1031 test showed p value < 0.0001 between *daGal4/+* and *da> Mtm* RNAi for *Mtm* and p value = 0.35
1032 between *daGal4/+* and *da> Mtm* RNAi for *CG3632*, and p value = 0.04 between *daGal4/+* and
1033 *da> Mtm* RNAi for *CG3530*.

1034 (B) (i) Representative confocal images of salivary glands from the genotypes a. *AB1Gal4/+*, b.
1035 *AB1>Mtm* RNAi. Cell body is marked majenta by BODIPY conjugated lipid dye, nucleus is
1036 marked by DAPI shown in green. Scale bar indicated at 50 μm .

1037 (ii) Graph representing average cell size measurement (in μm^3) as mean \pm S.E.M. of salivary glands
1038 from wandering third instar larvae of *AB1Gal4/+* (n = 7), *AB1> Mtm* RNAi (n = 7). Sample size is
1039 represented on individual bars. Student's unpaired t-test with Welch correction showed p value =
1040 0.0005.

1041 (C) Graph representing Normalised PI3P levels which is the peak area of GroPI3P/ peak area of
1042 GroPI4P normalised to organic phosphate value as mean \pm S.E.M. of *dal*⁺ (green) and *da*[>] *Mtm*
1043 RNAi (magenta). Biological samples = 4, where each sample was made from five third instar
1044 wandering larvae. Student's unpaired t-test with Welch correction showed p value = 0.07.

1045 (D) (i) Graph representing Atg8a punctae measurement in the salivary glands from wandering third
1046 instar larvae of *AB1>ATG8a-mCherry* (N =7, n =40), *AB1>ATG8a-mCherry; Mtm RNAi* (N =7,
1047 n =40). Student's unpaired t-test with Welch correction showed p value <0.0001.

1048 (ii) Representative confocal z-projections depicting autophagosomal levels using Atg8a-mCherry
1049 in the salivary glands from the genotypes a. *AB1>ATG8a-mCherry*, b. *AB1>ATG8a-mCherry; Mtm*
1050 *RNAi*. Scale bar indicated at 20 μ m.

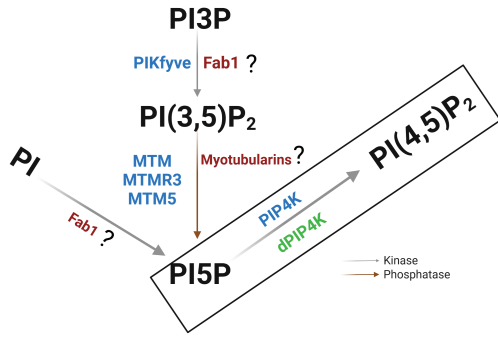
1051 (E) Graph representing average cell size measurement (in μ m³) as mean \pm S.E.M. of salivary glands
1052 from wandering third instar larvae of *AB1/+* (n = 11), *AB1>Mtm RNAi* (n = 8), *AB1>Mtm RNAi,*
1053 *Atg8a RNAi* (n = 12). Sample size is represented on individual bars. One way ANOVA with post
1054 hoc Tukey's test showed p value < 0.0001 between *AB1/+* and *AB1>Mtm RNAi* and p value =
1055 0.0002 between *AB1/+ ; dPIP4K²⁹* and *AB1>Mtm RNAi, Atg8a RNAi*.

1056 **Supporting Figure 6: PI3P regulates cell size in salivary glands**

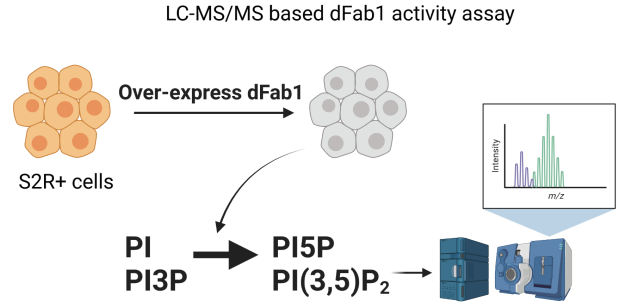
1057 (A) Graph representing average cell size measurement (in μ m³) as mean \pm S.E.M. of salivary glands
1058 from wandering third instar larvae of *AB1Gal4/+* (n = 7), *AB1> Mtm RNAi* (n = 7). Sample size is
1059 represented on individual bars. Student's unpaired t-test with Welch correction showed p value =
1060 0.009.

1061 (B) Immunoblot from the salivary glands of wandering third instar larvae probed using mCherry
1062 antibody showing the expression of Atg8a-mCherry in *AB1>ATG8a-mCherry* (control) and
1063 *AB1>ATG8a-mCherry; Mtm RNAi*. Atg8a-mCherry migrates ~42 kDa. Tubulin was used as the
1064 loading control.

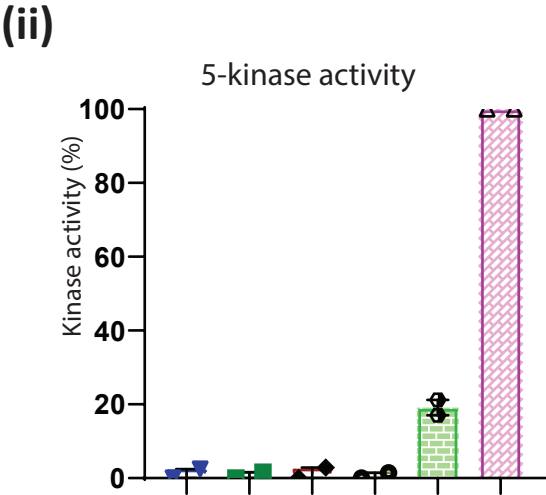
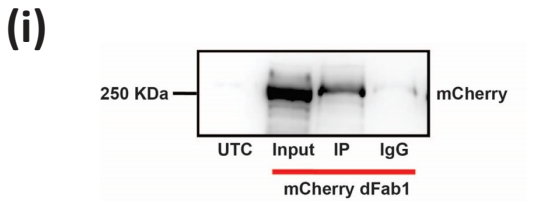
A



B

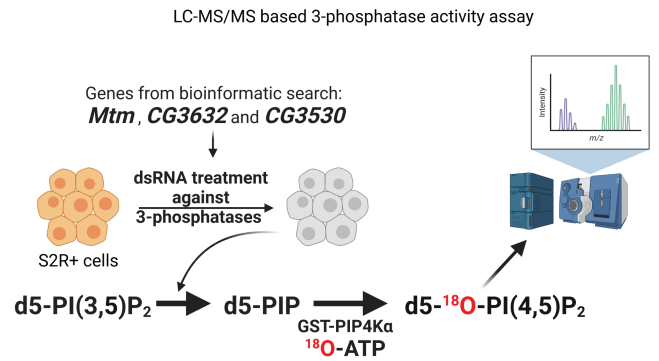


C

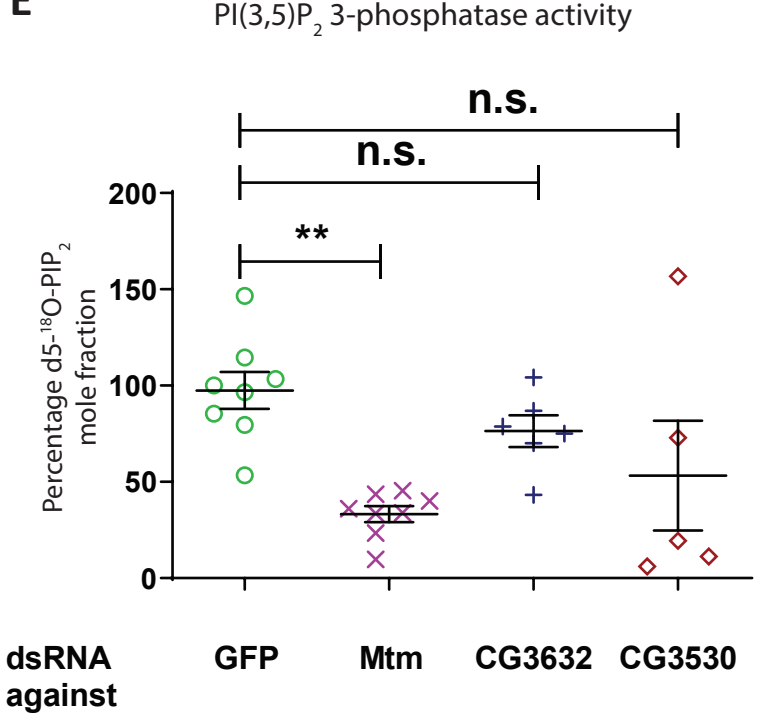


17:0 14:1 PI	+	-	+	-	+	-
17:0 20:4 PI3P	-	+	-	+	-	+
	No beads		Ctl beads		dFab1 beads	

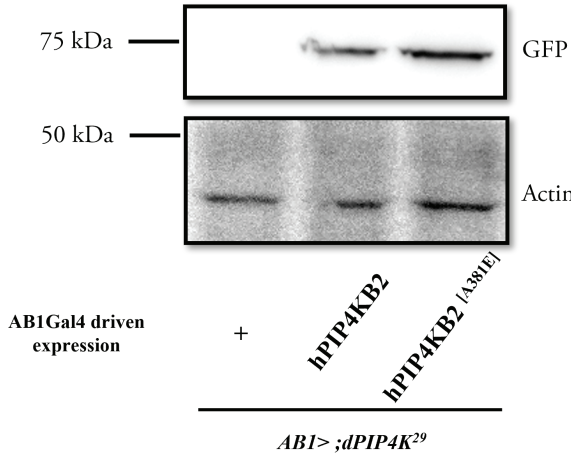
D



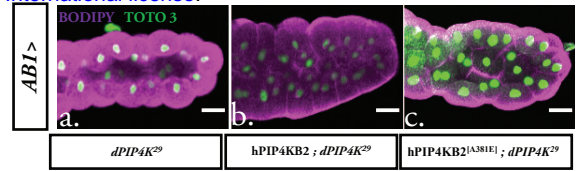
E



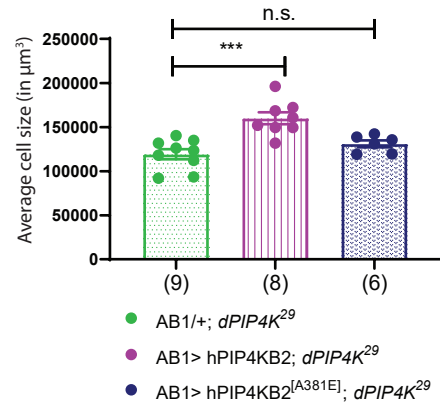
A



B



(ii)



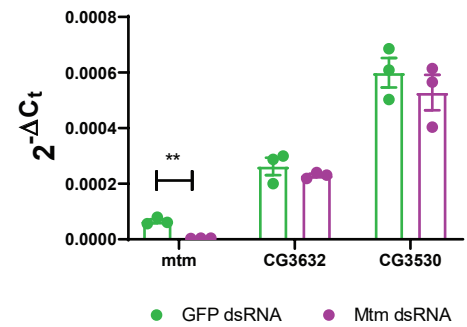
C

```

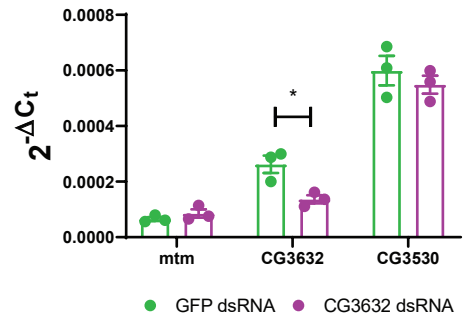
MTM1 331 ---NVESHWLSSLSTHWLBHIKLVLTGATQVADKVSSGKSSVLVHCSDGWDRTAOLTS
MTMR1 394 ---SIDEARWLSNVDGTHWLEYTRMLLAGARIADKESGKTSVVVHCSDGWDRTAOLTS
MTMR2 373 ---NIETHWLSNLESTHWLBHIKLLLAGARIADKVESGKTSVVVHCSDGWDRTAOLTS
MTMR3 369 ---MPDPGNWLSALESTKWLHHLSVLKSALLVHAVQDQRPVLVHCSDGWDRTAOLTS
MTMR4 363 ---MPDPSNWLSALESTKWLOHHSVMLKAALVANTVREGRPVLVHCSDGWDRTAOLTS
MTMR5 1412 AA-EPSPASELRSLEDSEWLIOCHKLLQVSVLWVELEDS-GSSVLVHCLEDGWDRTAOLTS
MTMR6 292 ---GLSVNDEYSGLESSSGLRHIKAVMDAAFLAKAMTVENASVLVHCSDGWDRTAOLTS
MTMR7 294 ---SPSMSDELWGLENSGLRHIKATMDAGFTIAKAVSEEGASVLVHCSDGWDRTAOLTS
MTMR8 294 ---TPTMSEELSGLESSSGLRHIKATMDAGFTIAKAVSEEGASVLVHCSDGWDRTAOLTS
MTMR9 289 ---THNMDRWLSRLEASNWLHIKRELTTACLAAOCTDREGASLLRGTHGSTLQVTS
MTMR10 359 ---EETEKWLSLENTRWLEYVRAFLKHSAELVYMLESSKHLSVLVCEBEGRDLSCCVAS
MTMR11 331 ---SVADKWLSALECTRWLDYVRACLRKASDISVLTSRVRSVTLQERGDRLINGLLSS
MTMR12 347 ---WDTIRWFSLLESSSWLDITRCLKKAEETETCMEAQNMNVLLEENASDLCCLISS
Mtm 353 ---TTDESKWQATNTLWLKHIRCLLAGARIVDKVFTMSTSVVHCSDGWDRTAOLTS
CG3632 436 ---SPDPPNYGQLEKTMWQELSGLGLNTVVVHTLEKNGRPVLVHCSDGWDRTAOLTS
CG3530 291 ---SPTMSARTNALESSGWLKHIRSTLDTSSFTANAVK-GVSVVHCSDGWDRTAOLTS
CG5026 354 ---GCSTDKWLSLENSGWLSLVLNSLNMSCVAOCLDQEGSPVLVHGAKGLDSTLIVIS
CG14411 423 EKFMLOQDKYLGLEKTNWLFYSLCLRYASEASATRS-GVLCVCESNGRDLCCVIS
    
```

D

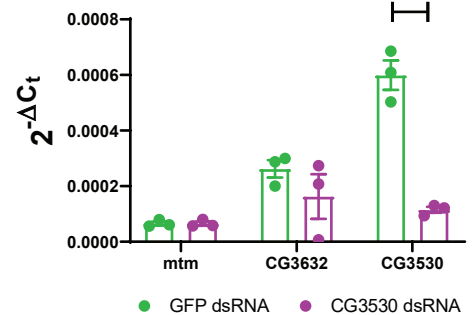
(i)

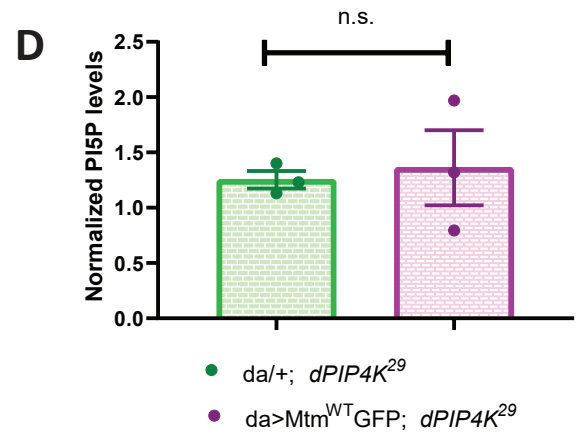
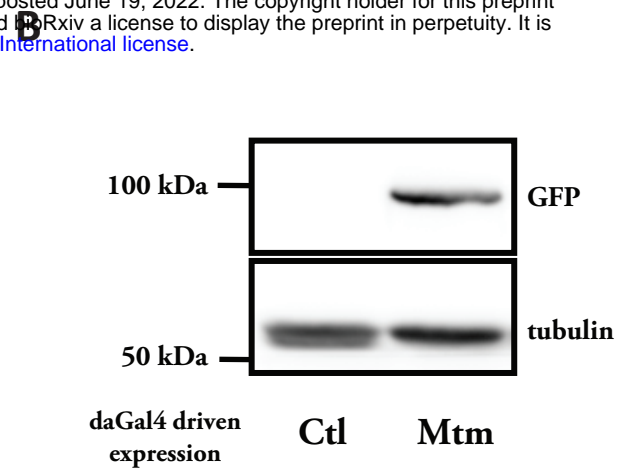
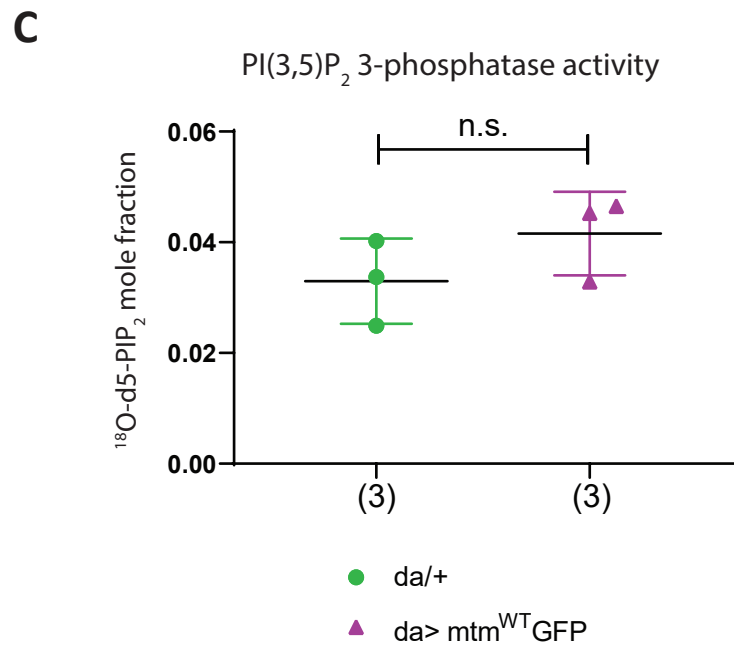
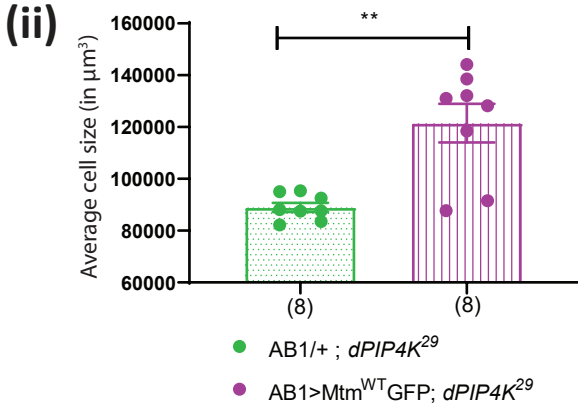
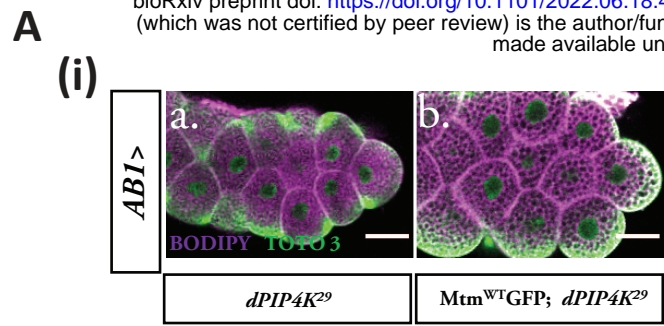


(ii)

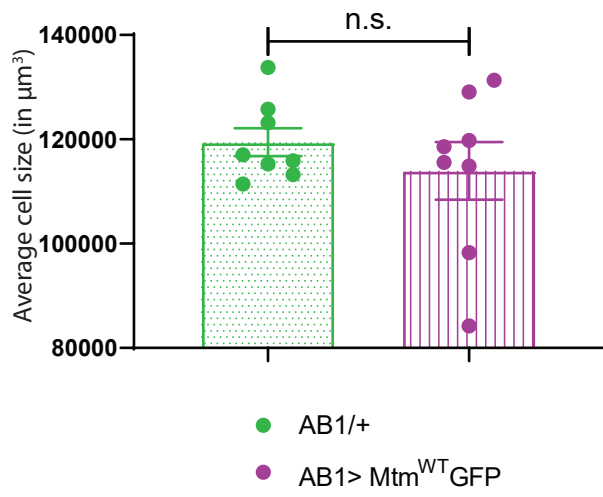


(iii)



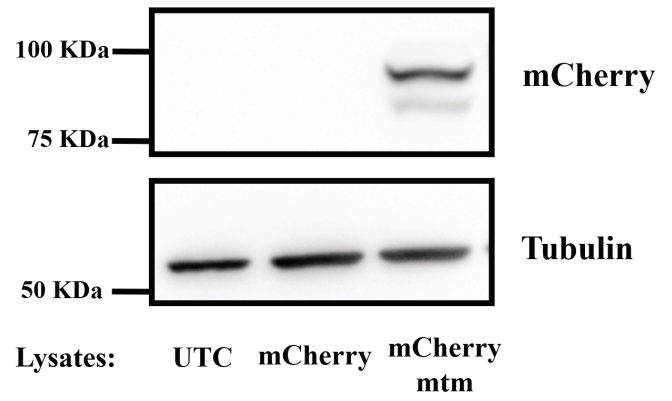


A

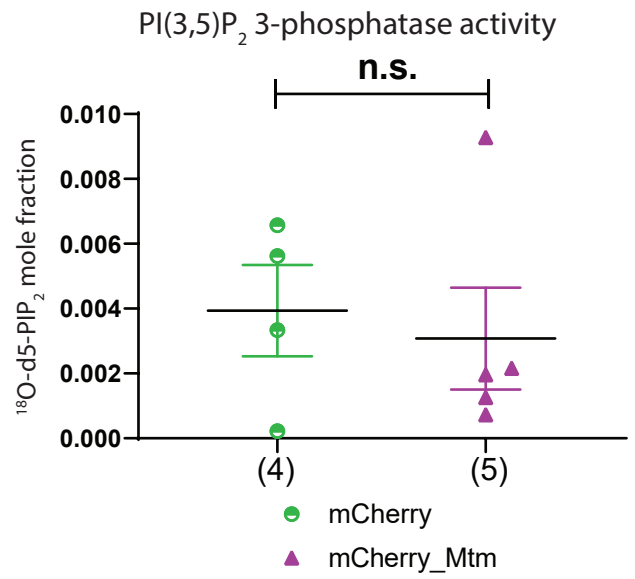


B

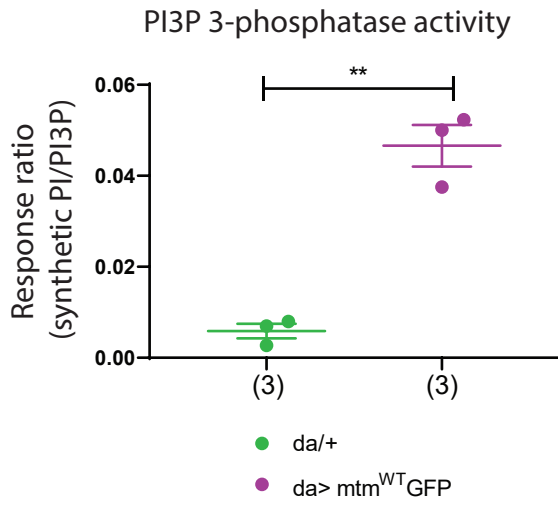
(i)



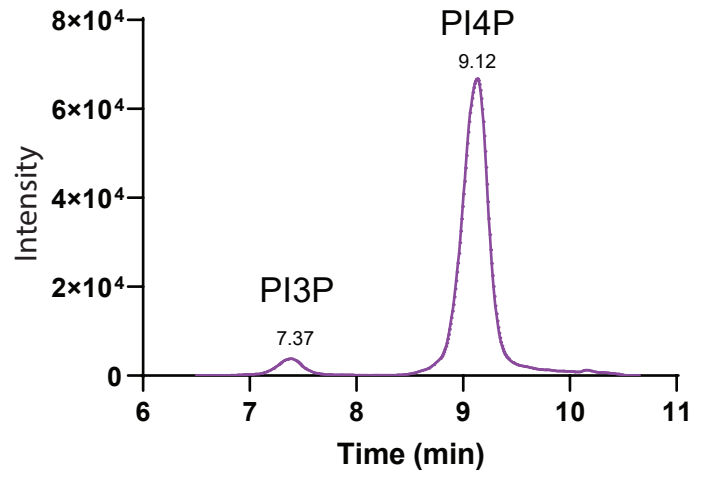
(ii)



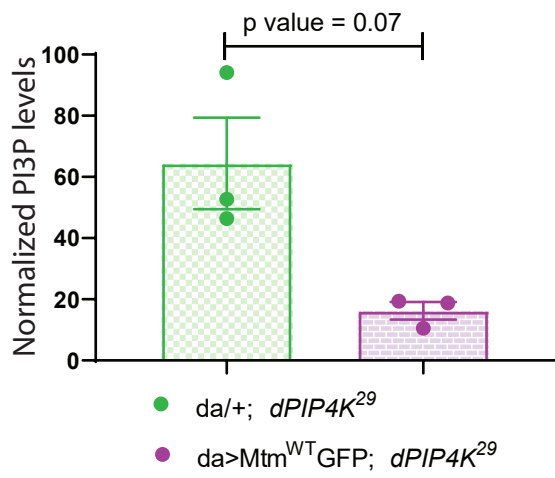
A



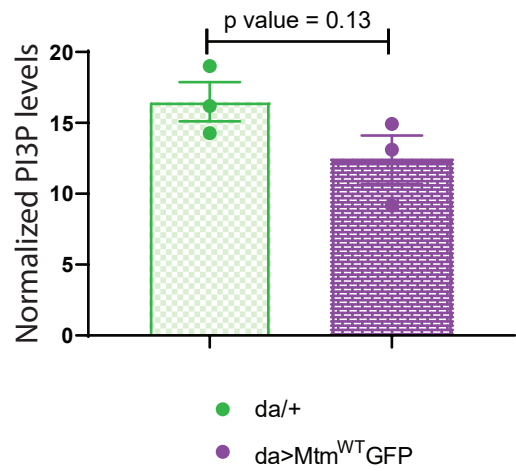
B

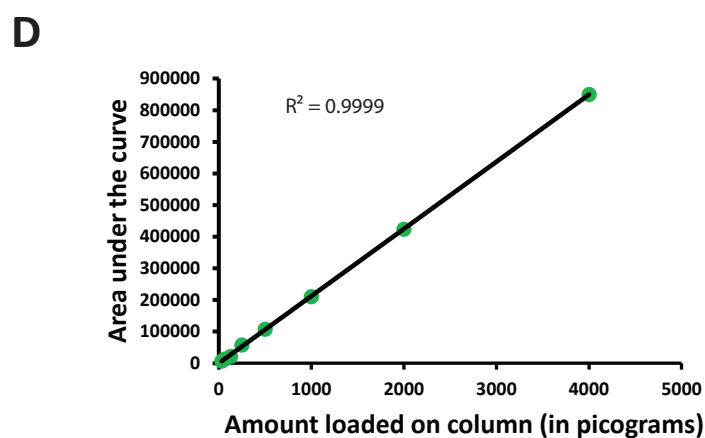
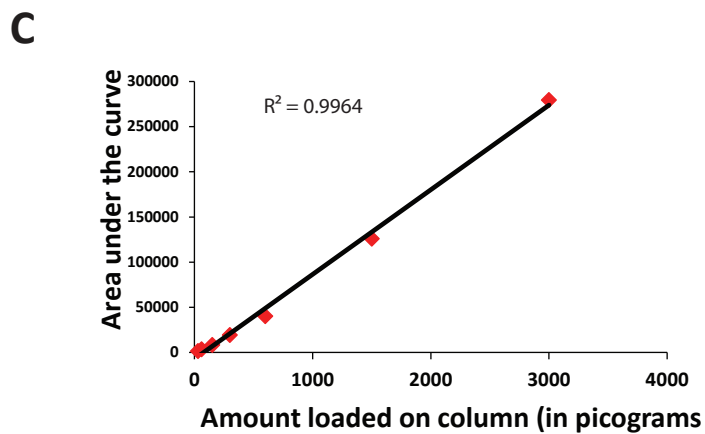
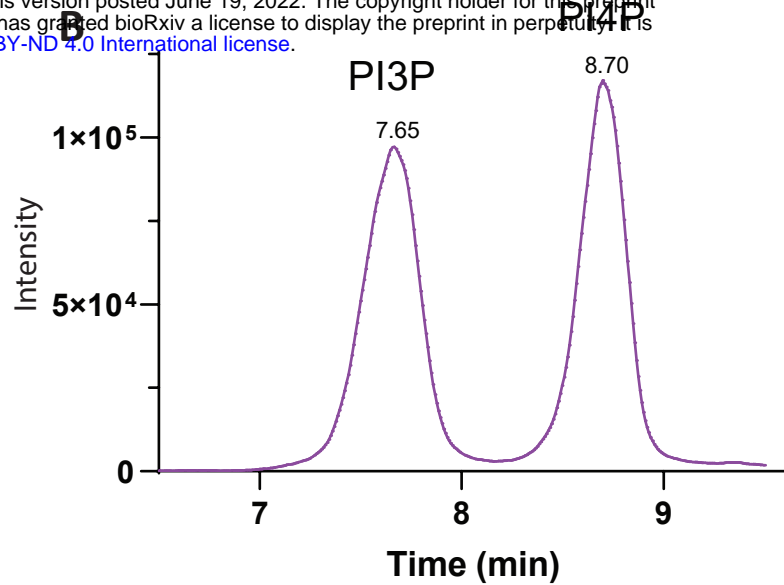
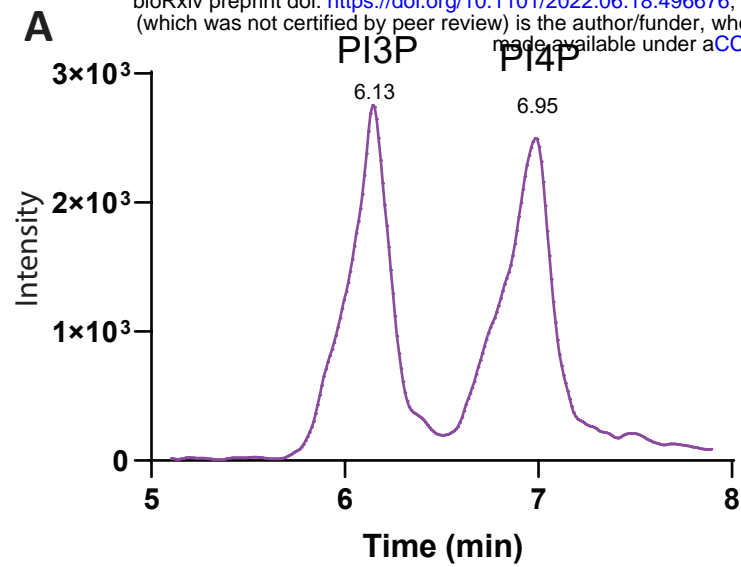


C

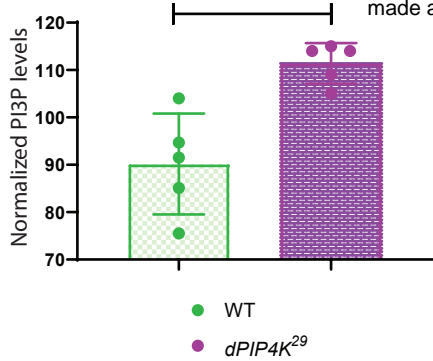


D

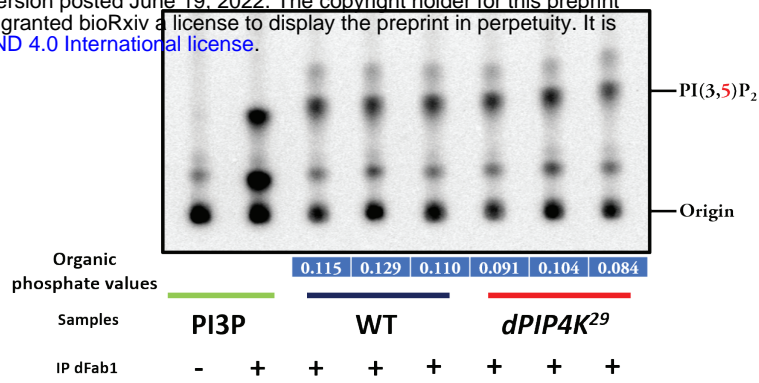




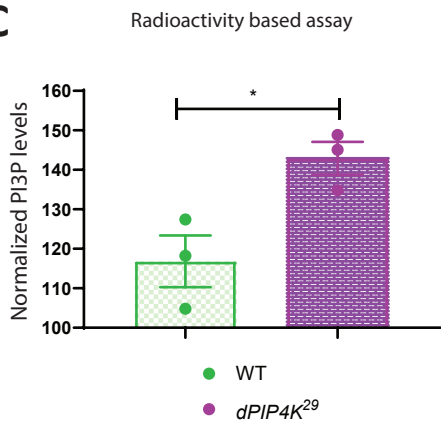
A



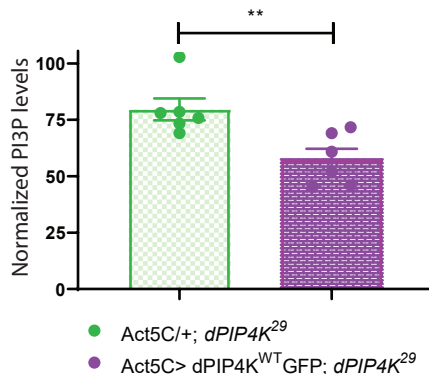
B



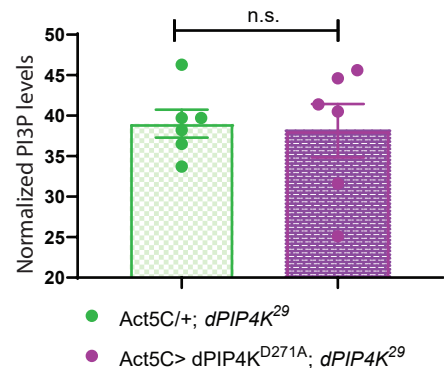
C



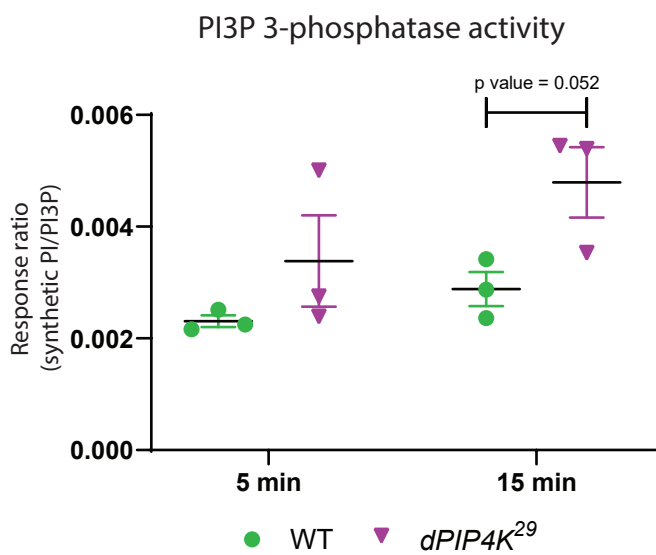
D



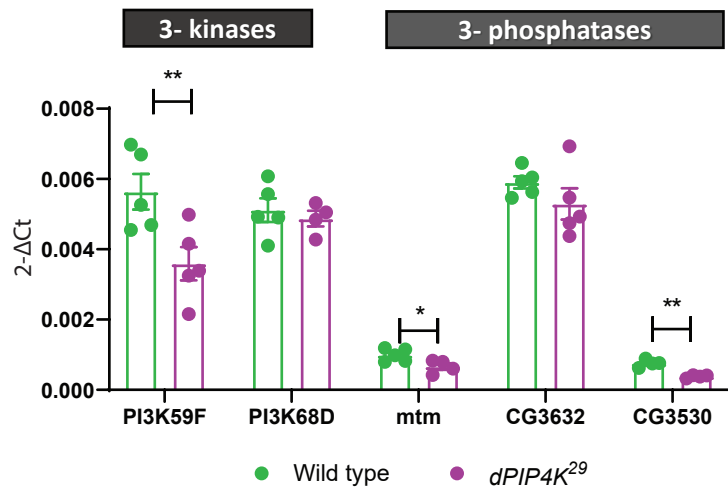
E



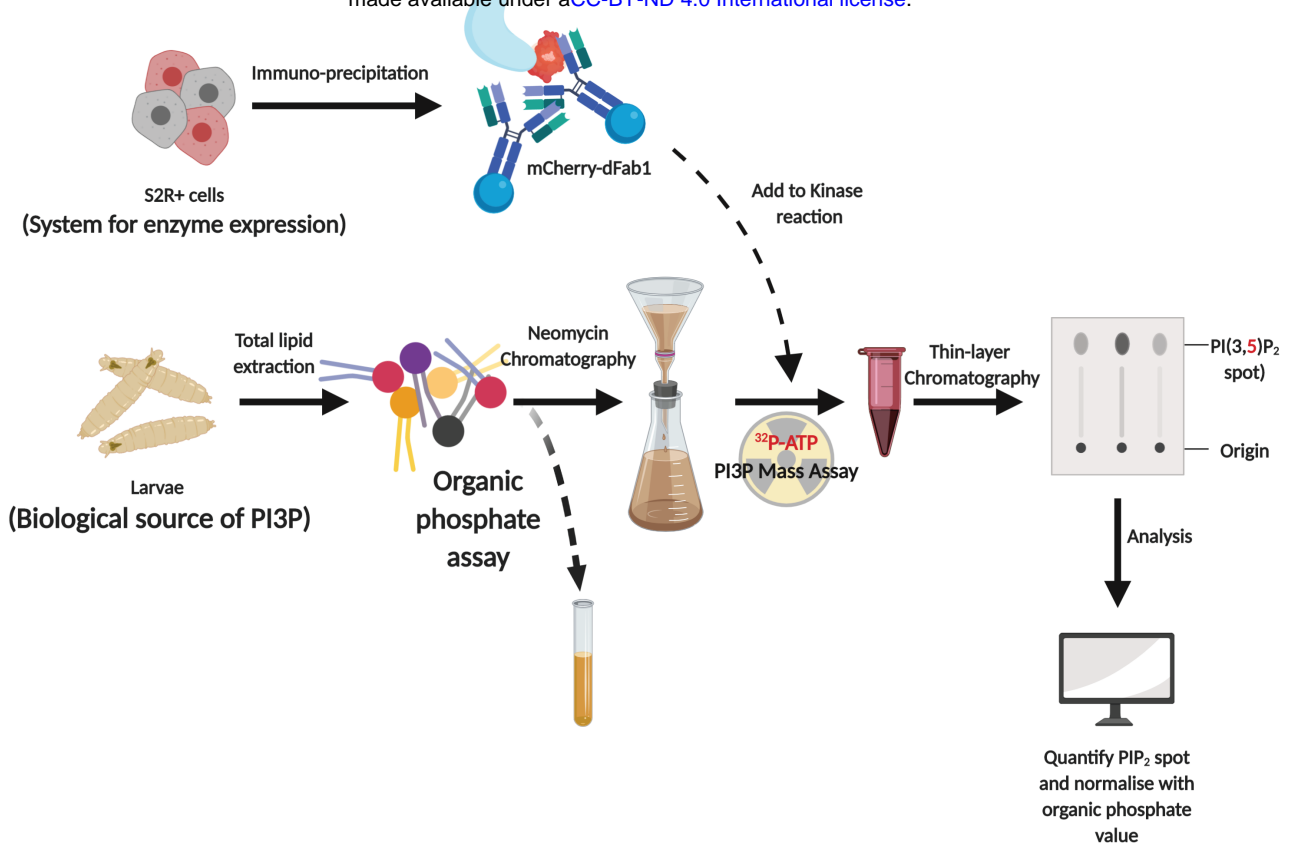
F



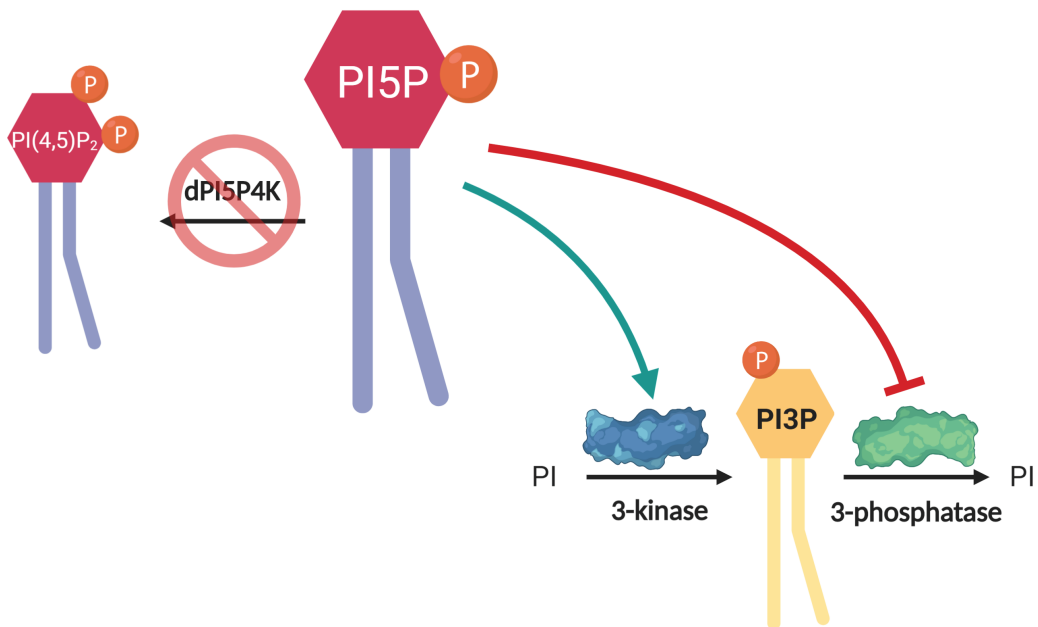
G



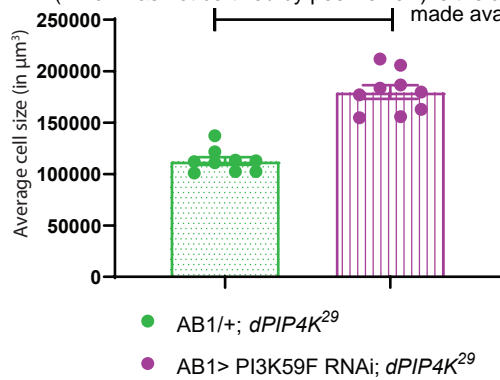
A



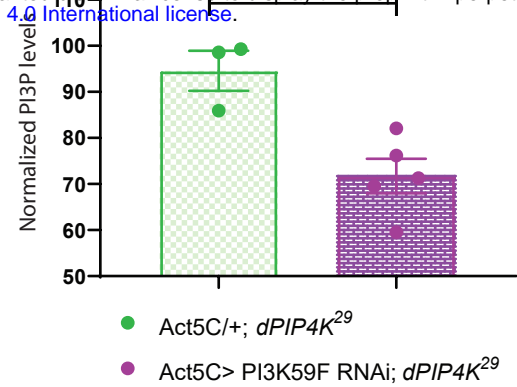
B



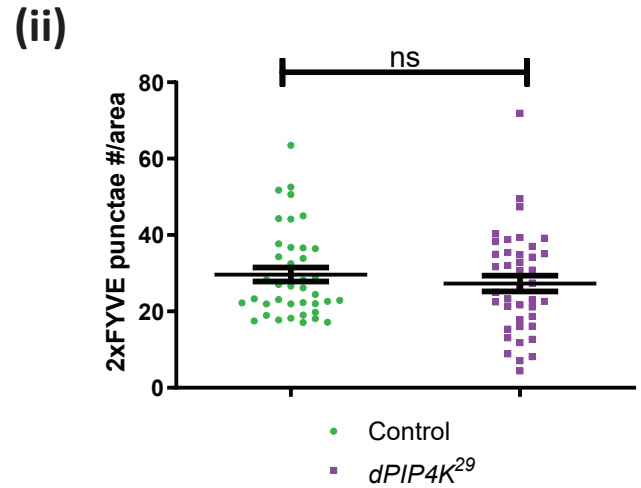
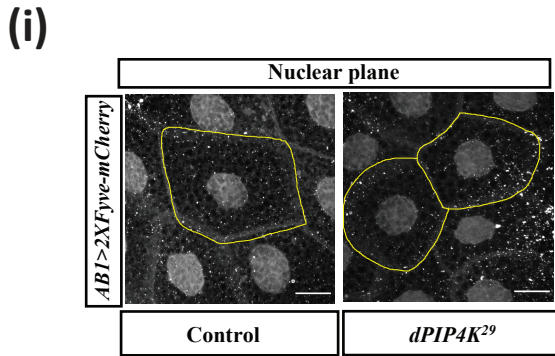
A



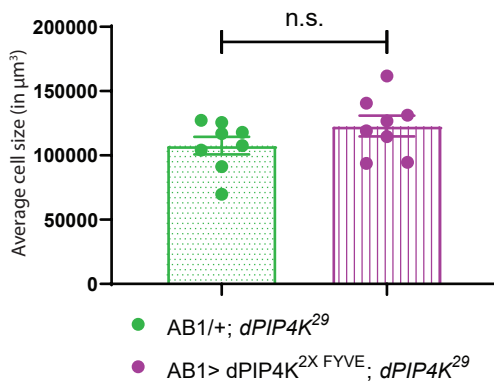
B



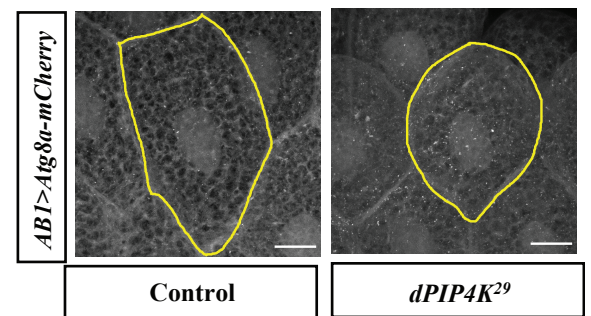
C



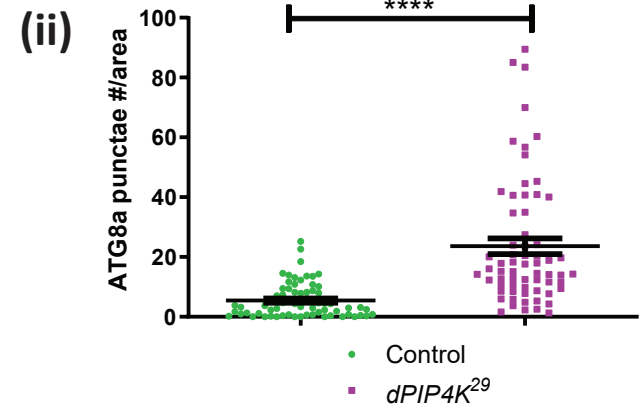
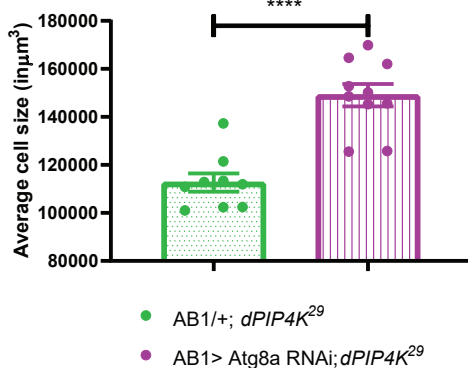
D



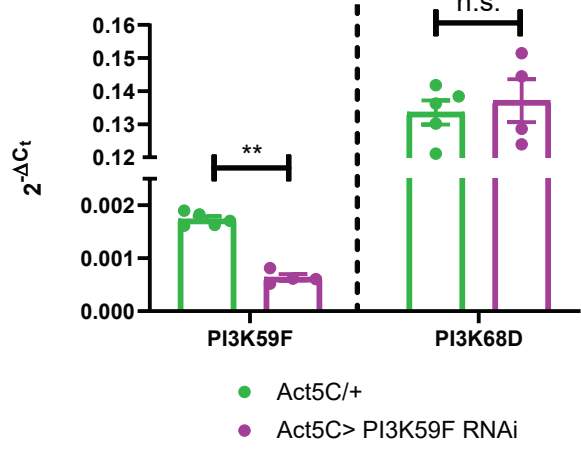
E



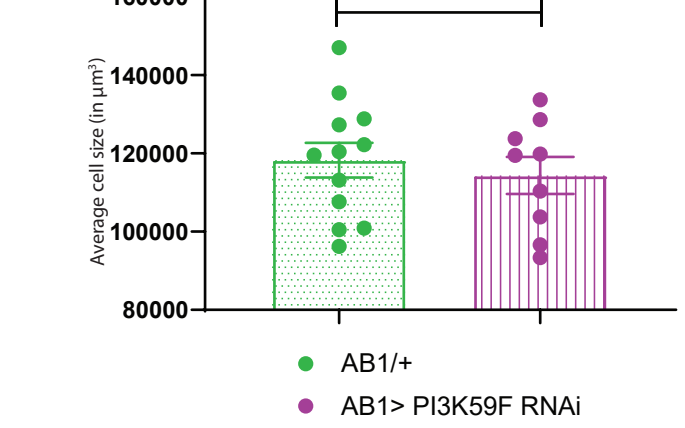
F



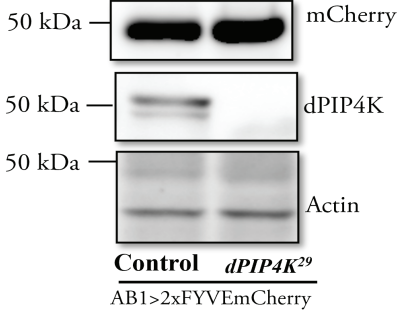
A



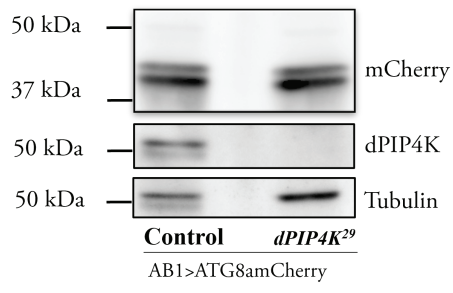
B



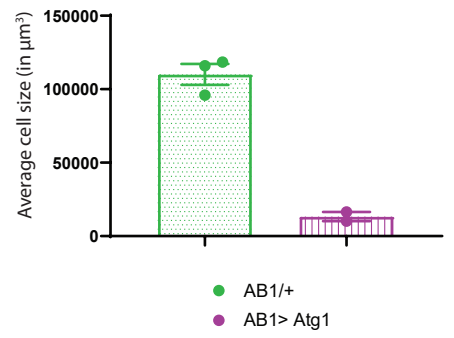
C



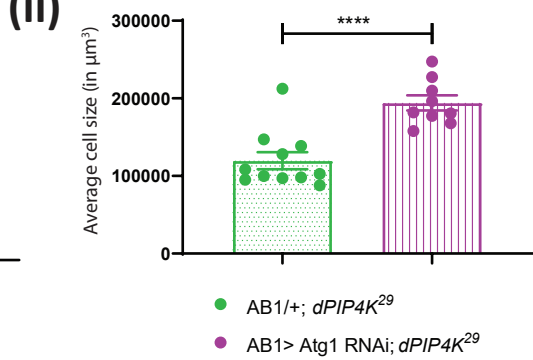
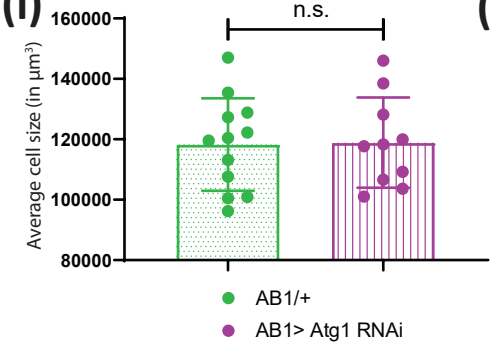
D



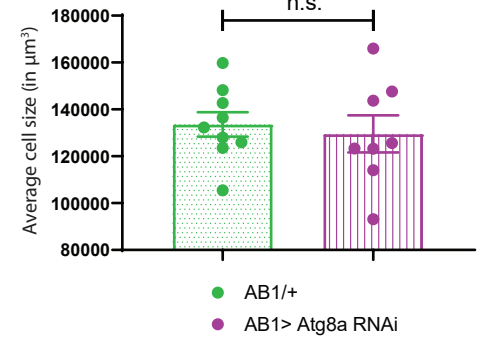
E



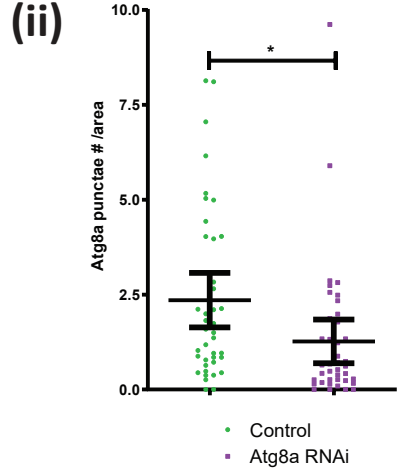
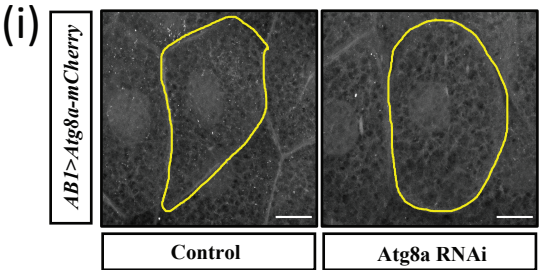
F



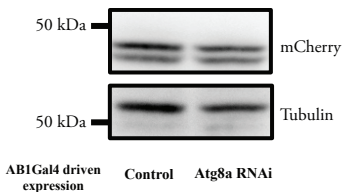
G

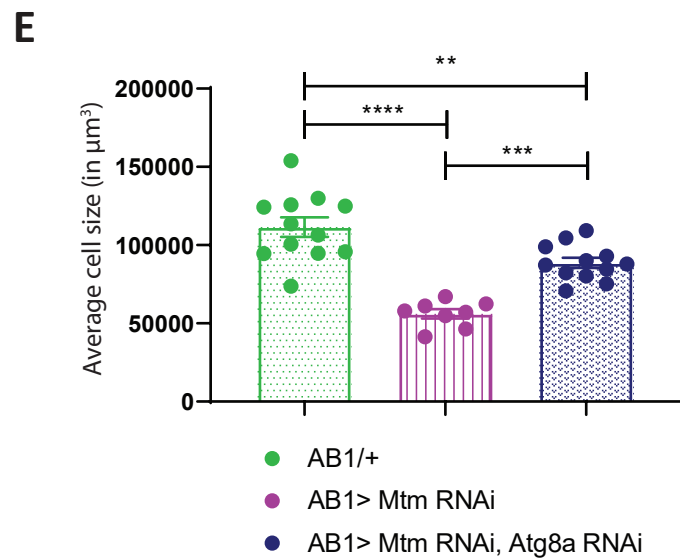
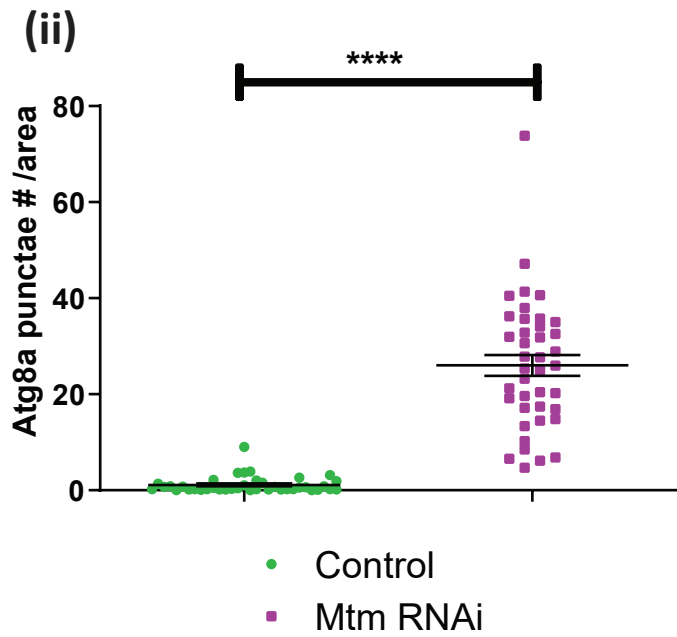
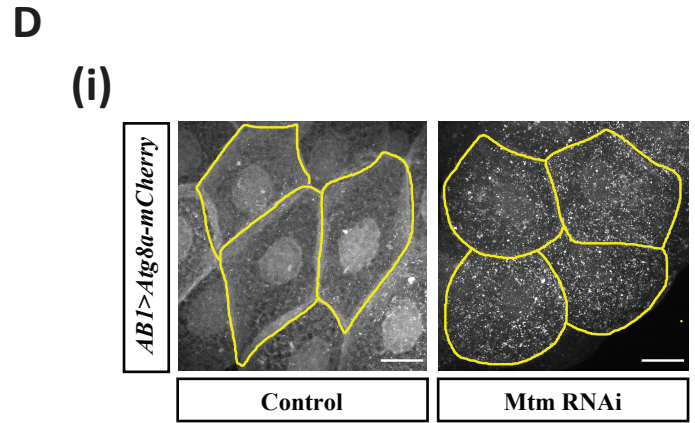
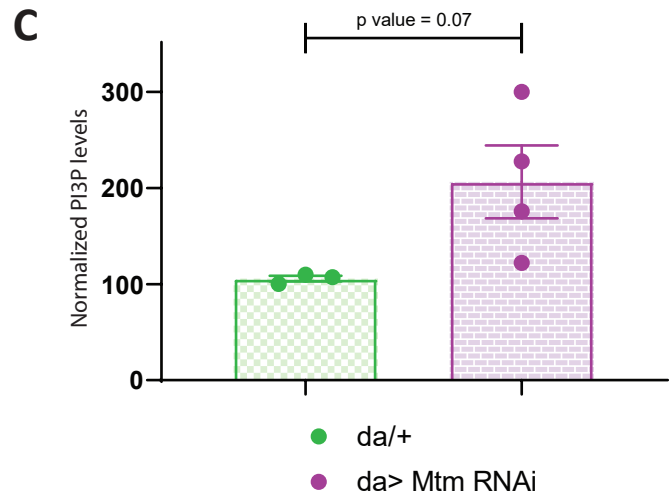
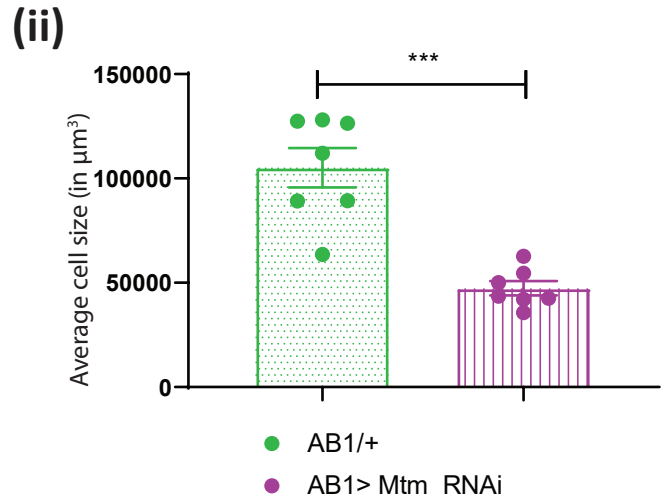
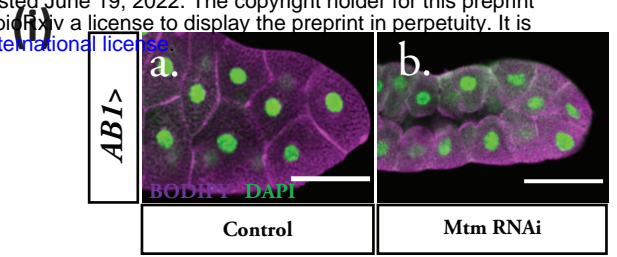
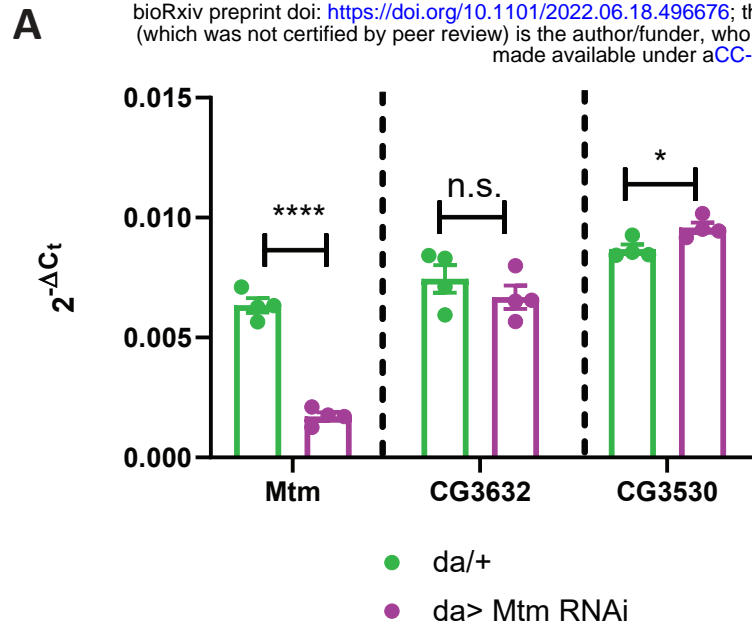


H

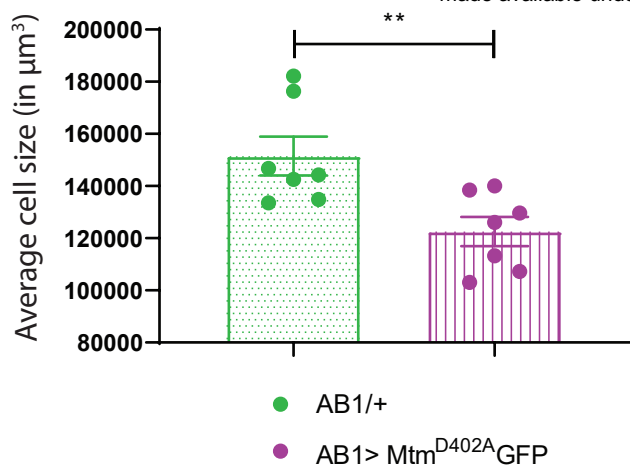


I





A



B

